A microscopic view of wood fibers, showing a dense network of dark grey and black fibers. Several prominent fibers are highlighted in a bright yellow color, creating a striking contrast against the darker background. The fibers are oriented in various directions, creating a complex, textured pattern.

ENERGY REDUCTION IN MECHANICAL PULPING

NOVEMBER 2023



THE UNIVERSITY OF BRITISH COLUMBIA

WELCOME MESSAGE

Dear partners in the Energy Reduction in Mechanical Pulping research program,



As we continue making progress in the fourth year of the program, I would like to present you our latest research project updates in preparation for our Fall 2023 Steering Committee meeting happening on November 2nd at UBC. We are looking forward to discussing progress and future work with you then.

During the past months, new faces have joined the program and we have also had some farewells. Dr. Kudzanai Nyamayaro has joined project 3.1 as a new postdoctoral fellow, Oren Han and Kasish Mahajan are our new COOP students working at the PPC and Joanne Wang joined us over the summer as a Mitacs Globalink student. In terms of farewell, our previous Ph.D. student, Juliana Lima de Freitas started a new position in Canfor Pulp as Senior Analyst for External Sustainability Reporting and our undergraduate students, Stephen Lee, Nilgun Abali and Farah Sadek ended their COOP term with us in August. We thank each one of them for their support in helping us meet our research objectives and we wish them great success in their future careers.

I encourage you to visit pages 35 to 37 for brief introductions to our new team members, with insights into their academic backgrounds and other updates on the program. The last pages of this newsletter summarize our team participation in different conferences and meetings over the past months.

Sincerely,

A handwritten signature in black ink that reads "Mark Martinez". The signature is written in a cursive, slightly slanted style.

Mark Martinez, Ph.D., P. Eng.,
Professor of Chemical and Biological Engineering, UBC
Principal Investigator, ERMP Research Program



CONTRIBUTORS

Matthias Aigner
Rodger Beatson
Sam Brown
Siwei Chen
Emily Cranston
James Drummond
Elisa Ferreira
Mariana Frias de Albuquerque
Vijay Kumar Pediredla
Runxin Lai
Mark Martinez
Lewis Mason
Gloria Noki
Kudzanai Nyamayaro
James Olson
Brent Page
André Phillion
Scott Rennecker
Norman Roberts
Henok Sahile
Laurel Schafer
Boris Stoeber
Heather Trajano
Nicole Ting
Daniela Vargas Figueroa
Anderson Veiga
Peter Wild
Adam Wu
Cameron Zheng

DESIGNER CONTACT

Program Manager
Daniela Vargas Figueroa
daniela.figueroa@ubc.ca
604-827-2390

UBC Pulp and Paper Centre
2385 East Mall Vancouver, BC V6T 1Z4

CONTENTS

RESEARCH UPDATES

System design, Sensors and Control

- 4 **PROJECT 1.1** - LC refining of mechanical pulp. Matthias Aigner, Samira Gharekhani, Mark Martinez, James Olson, Peter Wild. UVic and UBC
- 9 **PROJECT 1.2** - Data-driven control and analytics in the pulp and paper industry. Vijay Kumar Pediredla, Bhushan Gopaluni, Yankai Cao. UBC
- 13 **PROJECT 1.3** - Creating low-energy shive-free pulps. Claire Maulit, Rodger Beatson, Heather Trajano, Gloria Noki, Renz Po, Runxin Lai. BCIT & UBC

Valorization of TMP fines

- 18 **PROJECT 2.1** - Lignin-rich fines: Simple routes towards creation of hydrophobic and hydrophilic filler additives. Scott Rennecker, Siwei Chen, Adam Wu. UBC
- 25 **PROJECT 2.2** - From trees to treatment: Functionalizing TMP extractives. Cameron Zheng, Henok Sahile, Brent Page, Laurel Schafer, Heather Trajano. UBC
- 29 **PROJECT 2.3** - Production, characterization, and applications of MFC-derived from mechanical pulp fines. Mariana Frias de Albuquerque, James Olson, Heather Trajano, Boris Stoeber. UBC

New Product Development

- 33 **PROJECT 3** - Creating bulky fibres and advanced characterization through computed tomography. Anderson Veiga, Lewis Mason, Sam Brown, Elisa Ferreira, Kudzanai Nyamayaro, James Drummond, Emily Cranston, André Phillion, Mark Martinez. McMaster & UBC

PROGRAM UPDATES

- 36 **ERMP Personnel Updates**
- 37 **ERMP News**



ON THE COVER

On the cover, tracer fibres at micro scale visualized within handsheet samples using novel techniques of segmentation. The amber colour corresponds to tracer fibres and the grey colour corresponds to normal fibres. Author: Lewis Mason, MAsC student.

PROJECT 1.1

LC REFINING OF MECHANICAL PULP

Authors: Matthias Aigner, Samira Gharekhani, Mark Martinez, James Olson, Peter Wild

Background

In previous work by researchers at the University of Victoria, a custom piezo-ceramic force sensor was developed to measure local shear and normal forces applied to the refiner bars. Sensors based on this design have been used in trials in a variety of high consistency (HC) [Olender et al. 2008] and low consistency (LC) [Harirforoush et al. 2018] refiners. Most recently, trials were conducted at the Pulp and Paper Centre at UBC and at the Catalyst, Paper Excellence mill in Crofton, BC [Aigner et al. 2020, Aigner et al. 2022]. The goal of these studies was to investigate the effect of operating conditions on the radial distributions of bar-force, as characterized by the force profile during bar-passing events. From this work, new research questions emerged. Of particular interest in recent work is the impact of plate geometry on the refining process. The focus is specifically on understanding how key plate geometry parameters, including bar width and bar edge length (BEL), in conjunction with operating conditions like refiner speed and flow rate, influence critical pulp and handsheet properties, such as tear index and fiber length in the context of LC refining?

Experimental set up

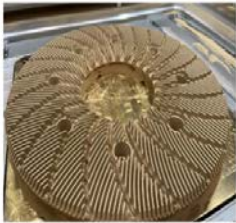


To expand on the previous findings of this research group, a comprehensive set of experiments was designed for and performed with the 16-inch AIKAWA single disc refiner at the PPC-UBC. The goal of these experiments is to investigate the effect of refiner plate geometry, such as bar width and BEL,

and refining parameters, such as specific edge load (SEL) and rotational speed, on bar force profiles and fiber and paper properties. The complete set of trials is intended to be a baseline study with potential to extend the knowledge of LC refining of mechanical pulp and aid in the development of new refiner plate designs.

The study uses three different refiner plates run at two rotational speeds and three levels of SEL, which results in a total of 18 trials. Table 1 presents a summary of the trial conditions. Note that Plates 1 and 2 have the same bar width while Plates 1 and 3 have the same BEL. This allows to investigate the impact of bar width and BEL on the refining process. These trials were completed in summer 2022.

Each trial is run in recirculation mode and fiber samples are taken at the no load position (S0) and at five times throughout each trial (S1-S5), with approximately equal accumulated Specific Refining Energy (SRE) between samples. Each fiber sample is analyzed on their fiber quality to determine fiber properties such as fiber length, fiber width and kink angle. Furthermore, handsheet test are conducted with each fiber sample to determine handsheet properties such as tensile strength and tensile index. These handsheet tests were completed in summer 2023. Similar to our previous work, a bar force sensor and a rotary encoder were installed on the refiner to record the bar forces and reference these to the position of the rotor with respect to the sensor. The force sensor and encoder sample continuously throughout each trial.

Table 1. Summary of the operating conditions for the pilot-scale LC refining trials.

	Plate 1 BEL: 2.1 km/rev Bar width: 1.4 mm	Plate 2 BEL: 5.4 km/rev Bar width: 1.4 mm	Plate 3 BEL: 2.1 km/rev Bar width: 2.5 mm
			
Rotational speed (RPM)	1200, 1600	1200, 1600	1200, 1600
SEL (J/m)	0.2, 0.4, 0.8	0.1, 0.2, 0.3	0.2, 0.4, 0.8
Consistency (%)	3.5	3.5	3.5
Flow rate (L/m)	250	250	250
Pulp type	Mechanical softwood pulp, Initial freeness 560 CSF, initial fiber length 1.45mm		

PROJECT 1.1

Results

Refining efficiency

Based on the handsheet tests, we can determine the refining efficiency for each plate. Refining efficiency, in this context, is defined as the increase in tensile index per unit of specific refining energy expended to achieve this increase, as outlined by Elahimehr et al. [Elahimehr et al. (2015)]. For a thorough analysis, we plot this efficiency against a measure of refining intensity. In this study, we utilize the ratio of net power to rotational speed as an indicator of refining intensity as a means of comparison across all trials. The resulting data, illustrating refining efficiency in relation to intensity, is presented in Figure 1.

Figure 1 includes all the data gathered in the current study. Each data point corresponds to the mean refining efficiency from its trial and is labeled with the refining conditions for that trial. Error bars based on the standard error measured from the mean refining efficiency within each trial, accompany these data points, serving as visual indicators for the degree of variability within each trial.

In general, there is a noticeable decrease in refining efficiency as the refining intensity increases. Upon closer examination of

the data for each plate and the two rotational speeds, it becomes evident that higher RPM results in superior efficiency for the same intensity level for Plates 1 and 3 but not for plate 2.

For Plate 1, the trial conducted at low power and at 1600 RPM, demonstrates the highest overall refining efficiency. In contrast, the same plate run at 1200 RPM exhibits significantly lower efficiency, consistent with the overall efficiencies observed for other plates at either rotational speed.

For Plate 3, the trial with the highest efficiency was at 1600 RPM and at a specific edge load (SEL) of 0.4, indicating a medium intensity. For Plate 2, the trial with the highest efficiency is associated with a low intensity trial run at 1200 RPM.

Extrapolating peak refining efficiency points for each plate from this plot suggests peak efficiency for Plate 1 at low intensity but high RPM, for Plate 2 at an even lower intensity but at 1200 RPM, and for Plate 3 at medium intensity and again at 1600 RPM.

The analysis of refining efficiency concerning refining intensity reveals that while there are similarities in the trends for the three plates, the efficiency behaves differently for each plate with respect to rotational speed and intensity. This variation is attributable to the distinct plate geometry parameters of each plate.

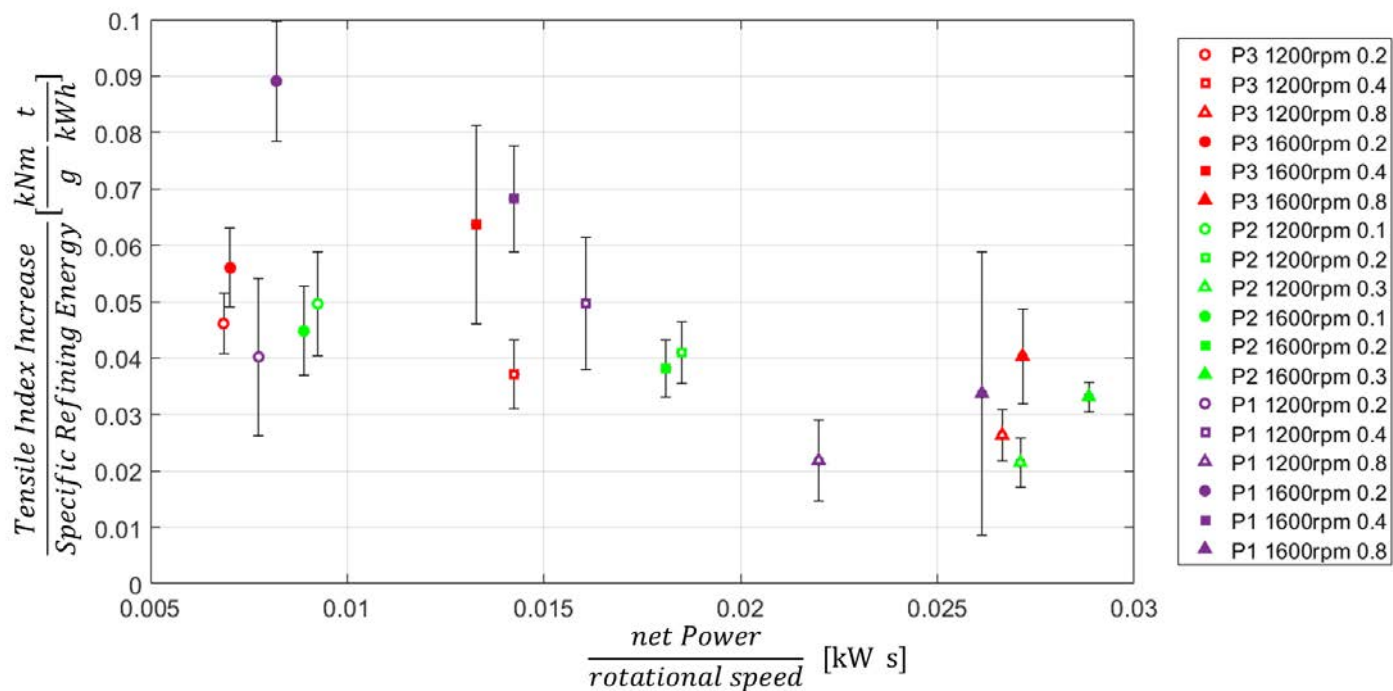


Figure 1. Refining efficiency data for all 18 trials conducted in the baseline study. The horizontal axis corresponds to refining intensity, calculated as the ratio of net power to rotational speed, while the vertical axis illustrates the increase in tensile index per unit of specific refining energy applied to increase the tensile index. Each trial is identified by its associated plate number, rotational speed, and specific edge load.

Plate geometry

A method was established to measure specific plate parameters from images, drawing inspiration from the work of Elahimehr et al. [Elahimehr et al. (2015)]. This process is delineated in Figure 2. Utilizing images of the refiner plates (Figure 2 (a)), binary images are generated for the rotor side and for the stator side (Figure 2 (b) and 2 (c)). These binary images are then used to identify the areas of overlap between the stator bars and the rotor bars during the refining process (Figure 2 (d)). Each of these overlapping areas is measured and documented, serving as the basis for deriving novel plate geometry parameters, including the total overlap area, the number of contacts, the edge length, and the open volume.

The total overlap area represents the sum of all the overlapping areas between the rotor and stator patterns. The number of contacts is representing the number of instances of overlap between the rotor bars and stator bars. Edge length is calculated as half of the perimeter of each overlap area and is intended to represent the edge length of each element facing into the direction

of rotation. Finally, the open volume refers to the space on the rotor plate enclosed by the refiner bars.

In Figure 3, we compare the new plate geometry parameters with the BEL. Note that Plate 1 and Plate 3 share the same BEL, yet Plate 3 exhibits an overlap area nearly three times larger than that of Plate 1. Furthermore, Plate 2, with a BEL higher than Plates 1 and 3, features a smaller overlap area than Plate 3 but greater overlap than Plate 1.

Shifting focus to edge length, Plate 3 has double the edge length of Plate 1, while Plate 2 exhibits almost three times the edge length of Plate 1. In terms of the number of contacts, Plates 1 and 3 share a similar count, while Plate 2 stands out with a significantly higher number. Notably, open volume displays an inverse relationship with edge length, with Plate 1 featuring the largest open volume and Plate 2 having the smallest.

From this analysis, it is apparent that BEL represents a similar relationship between the plates as the number of contacts between the rotor and stator bars. In contrast, BEL does not provide insight into total overlap area, edge length or open volume.

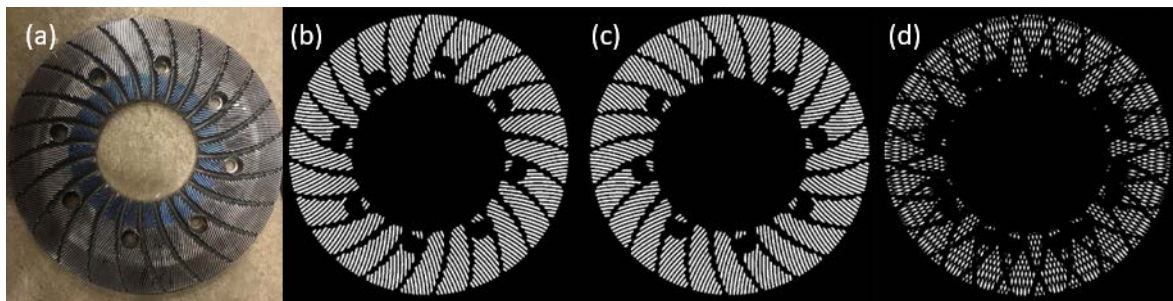


Figure 2. Plate geometry pipeline. (a) Picture of a refiner plate. (b) Black and white image of a stator plate (c) and a rotor plate. (d) Bar interaction area image generated using (b) and (c).

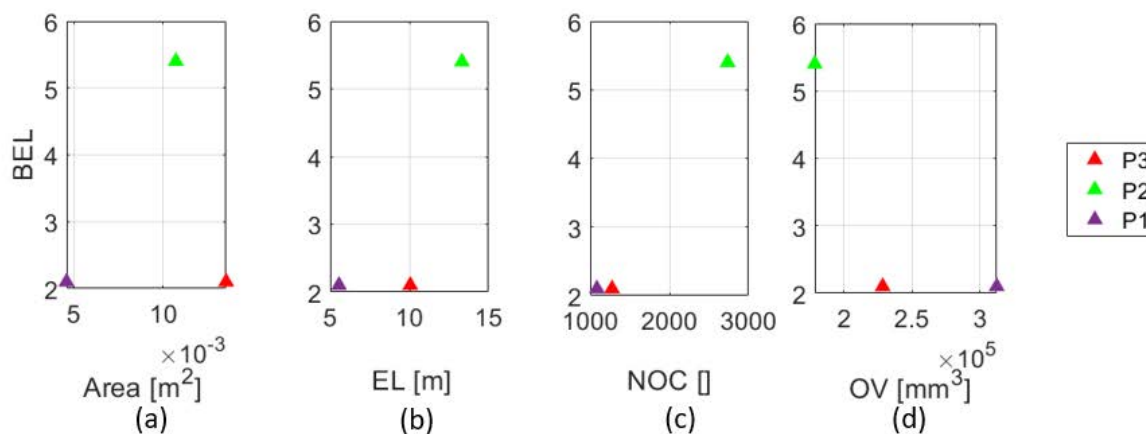


Figure 3. Comparison of bar edge length with measured plate geometry parameters, (a) total area of the bar interaction elements (area), (b) edge length (EL) of the bar interaction area, (c) number of bar interaction elements (NOC) and (d) open volume (OV) on the rotor plate enclosed by the refiner bars.

PROJECT 1.1

Non-dimensional power

In an effort to establish a connection between power and plate parameters, we conducted a non-dimensional analysis. In this analysis, we calculated a dimensionless power based on Elahimehr et al. (Elahimehr et al. 2013) utilizing the net power, P_{net} , the water density, ρ , rotational speed, ω , and the refiner's radius, R , as indicated by Equation 1.

$$P_d = \frac{P_{net}}{\rho \omega^3 (2R)^5} \quad (1)$$

Similarly, we created a dimensionless plate parameter, denoted as g_d . This dimensionless value is calculated following Equation 2, using the plate gap, gap , refiner radius, R , as well as previously defined parameters edge length, EL , and overlap area, $area$.

$$g_d = \frac{gap}{R} \frac{R}{EL} \frac{area}{R^2} \quad (2)$$

The overarching objective here is to identify a relationship between plate geometry and power required, and vice versa. The two dimensionless values are graphically represented in Figure 4. The notable outcome is that, regardless of plate geometry or the level of refining, we can predict the power associated with each plate gap. This represents a significant enhancement compared to earlier models such as presented by Elahimehr et al. [Elahimehr et al. (2013)], which relied primarily on bar geometry parameters such as bar width, groove width, and BEL. The improvement lies in the inclusion of novel plate geometry values in the predictive framework.

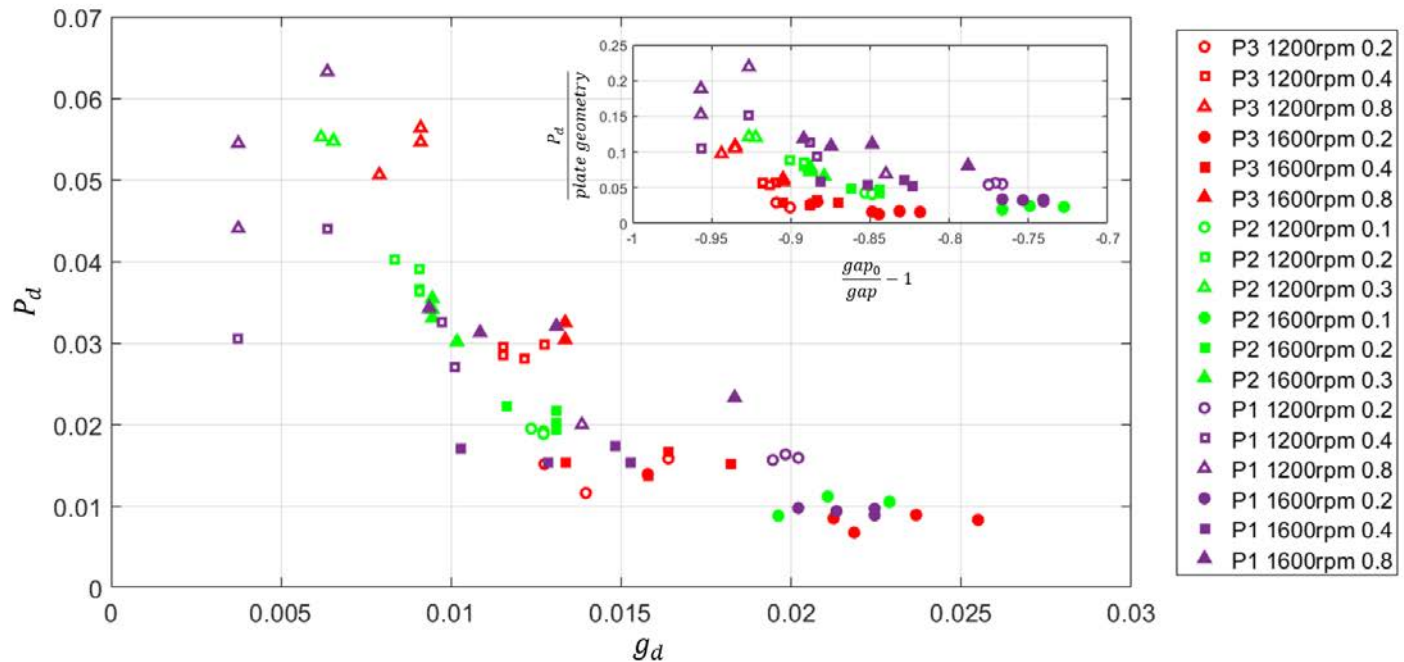


Figure 4. Non-dimensional power plotted against non-dimensional gap including measured plate geometry parameters (edge length and interaction area). Inset presents earlier model presented by Elahimehr et al. [Elahimehr et al. (2013)]. The vertical axis is comprised of the dimensionless power divided by the plate geometry factor based on bar width and groove width while horizontal axis represents the dimensionless gap group.

Acknowledgements

The authors thank Mr. Norm Roberts for conducting the refining trials and the co-op students at the UBC-PPC for their hard work in analysing the fibre data.

References

1. Aigner, M., Olson, J., and Wild, P. (2020). Measurement and interpretation of spatially registered bar-forces in LC refining. *Nordic Pulp & Paper Research Journal*, 35(4), 600-610.
2. Aigner, M., Olson, J., Sun, Y., and Wild, P. (2022). Interpretation of force profiles in mill-scale LC refining. *Nordic Pulp & Paper Research Journal*, 37(1), 42-53.
3. Elahimehr, A., Martinez, D.M., Olson, J. A. (2012): A Method for Estimating the Area of Intersection Between Refiner Plates. *J. Powder Technol.*, (February 2012), 1-18.
4. Elahimehr, A., Olson, J. A. and Martinez, D. M. (2013): Understanding LC refining: The effect of plate pattern and refiner operation, *Nord. Pulp Pap. Res. J.*, 28(3), 386-391.
5. Elahimehr, A., Olson, J. A. and Martinez, D. M. (2015): Low consistency refining of mechanical pulp: how plate pattern and refiner operating conditions change the final properties of pulp, *Nord. Pulp Pap. Res. J.*, 30(4), 609-616.
6. Harirforoush, R, Olson, J., and Wild, P. (2017). In-Process Detection of Fiber Cutting in Low Consistency Refining Based on Measurement of Forces on Refiner Bars. *Tappi Journal* 16 (4): 460-69.
7. Olender, D., Wild, P., & Byrnes, P. (2008). A piezoelectric force sensor for mill-scale chip refiners. *Proceedings of the Institution of Mechanical Engineers, Part E: Journal of Process Mechanical Engineering*, 222(2), 115-122.

PROJECT 1.2

DATA-DRIVING CONTROL AND ANALYTICS IN THE PULP AND PAPER INDUSTRY

Authors: Vijay Kumar Pediredla, Bhushan Gopaluni, Yankai Cao

Background

Thermomechanical pulping (TMP) processes are widely used for newsprint productions owing to their relatively high pulp yield. However, the mechanical pulping process is also highly energy intensive, and the paper and pulp industry is ranked fourth among all industries in total greenhouse gas emissions. Also, due to the increase in electricity prices, environmental concerns, and low energy efficiency, the research focuses on energy consumption optimization while maintaining the expected pulp quality.

Artificial Intelligence (AI) and Machine Learning (ML) are increasingly being leveraged in the paper and pulp industry to enhance operational efficiency, reduce waste, and improve product quality. In this dynamic sector, AI-driven predictive maintenance is playing a pivotal role. By analyzing sensor data from critical machinery, AI models can predict when maintenance is required, preventing costly unplanned downtime. This not only improves the overall productivity of paper mills but also extends the lifespan of expensive equipment. Additionally, AI-driven quality control systems are transforming the production process. ML models can continuously monitor and analyze the quality of paper products, identifying defects in real-time. This ensures that only high-quality products reach the market, reducing waste and minimizing the environmental impact.

Furthermore, AI is revolutionizing supply chain management in the paper and pulp industry. Machine Learning algorithms analyze historical data and current market conditions to optimize inventory management and distribution. By accurately forecasting demand, companies can reduce excess stock and avoid stockouts. This streamlines the supply chain, cuts costs, and ensures that products are available when needed. In the realm of sustainability, AI is helping the industry become more eco-friendly. By monitoring energy consumption, AI models can identify areas of waste and recommend energy-saving measures, reducing the environmental footprint of paper manufacturing. These advancements are not only making the paper and pulp industry more competitive but are also aligning it with the growing global focus on sustainable production and resource management.

Summary of the work done

Process Operation Evaluation and Model Reliability Assessment for Pulping Process

In the continuous TMP process, aiming at improving energy efficiency and maintaining the produced pulp quality, a non-intrusive operating recommendation system is proposed with an extensible framework. This system uses a high-dimensional visualization technique based on the Kiviat diagram to integrate the multi-dimensional process operating space and the product quality. Simple and robust model structures are employed with sufficient accuracy, and intuitive illustrations of the process operating conditions with comprehensible statistics are provided for real-time implementation. The proposed Work links the process operating space to the intermediate pulp properties, controlled to regulate the handsheet properties, as shown in Figure 1 (a). To further investigate the relationship between pulp properties and the handsheet properties, an inferential sensor model was developed with a reliability index to indicate which input sample area is more likely to provide more accurate predictions.

Deep learning-based hybrid reconstruction algorithm for fibre segmentation from 3D X-ray images

3D X-ray tomography is a powerful scanning technique for generating images of complex fibre structures. A novel machine-learning algorithm to identify and separate individual fibres using 3D images is proposed in this article. The developed four-step hybrid 3D fibre segmentation algorithm involves deep-learning aided semantic segmentation that slices 3D images to create 2D images for fibre extraction, elliptical contour estimation combined with the marker-controlled watershed algorithm for separating fibres, identifying individual fibres through 3D reconstruction, and lastly, the 3D object refining approach, as shown in Figure 1 (b). The proposed methodology is implemented on a real-time sample of nylon fibre bundle under compression and its 3D X-ray image volume to validate the performance. The results show its superior performance compared to off-the-shelf image processing algorithms in terms of precision, with a validation accuracy greater than 90% and efficiency, preventing the need for a huge data set and reducing the complexity.

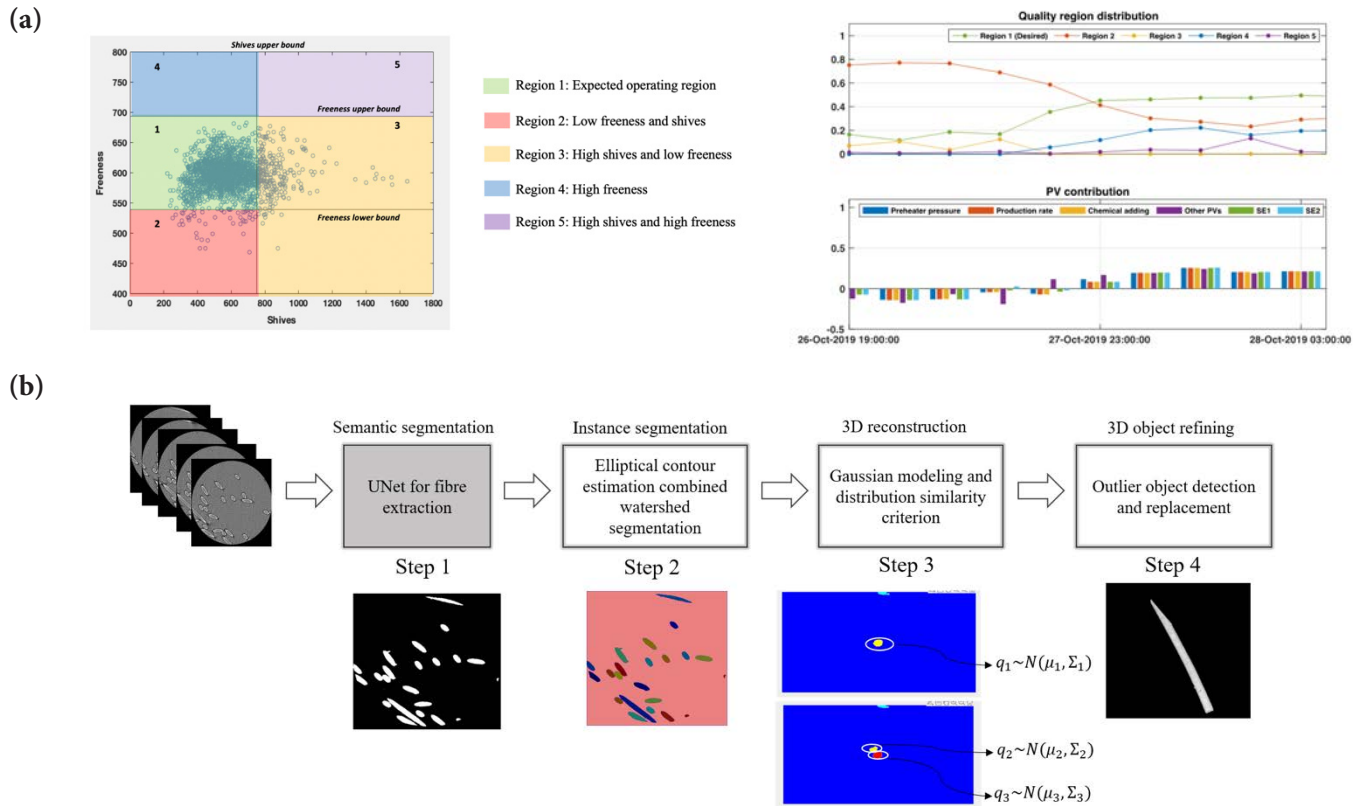


Figure 1. (a) Pulp property segmentation and process variable contribution indices. (b) Workflow of the deep-learning-based hybrid reconstruction algorithm for fibre segmentation

Reinforcement-learning-based Model Predictive Control

Model Predictive Control (MPC) has found significant application within the paper and pulp industry, transforming how manufacturing processes are managed. In this dynamic sector, MPC is employed to optimize various aspects of production, from pulping and chemical processes to paper machine operations. By utilizing real-time data, such as pulp consistency, machine speeds, and quality measurements, MPC algorithms predict the future behavior of the process and calculate optimal control actions. These actions are continually adjusted to minimize deviations from quality standards, reduce energy consumption, and maximize throughput. This fine-tuned control enhances the overall efficiency of the paper and pulp manufacturing process, reducing waste and lowering operational costs.

Moreover, in the pulp and paper industry, where the environmental footprint is a growing concern, MPC plays a crucial role in sustainability efforts. It allows for the precise management of chemical additives and water usage, helping mills minimize their environmental impact. Additionally, MPC is instrumental in predictive maintenance strategies. By continuously monitoring the condition of critical equipment, such as digesters and refiners, MPC can predict when maintenance is needed, reducing costly downtime and extending the lifespan of machinery. Overall, MPC has become a cornerstone technology in modern paper and pulp manufacturing, ensuring not only operational excellence but also supporting the industry's commitment to sustainability and resource efficiency.

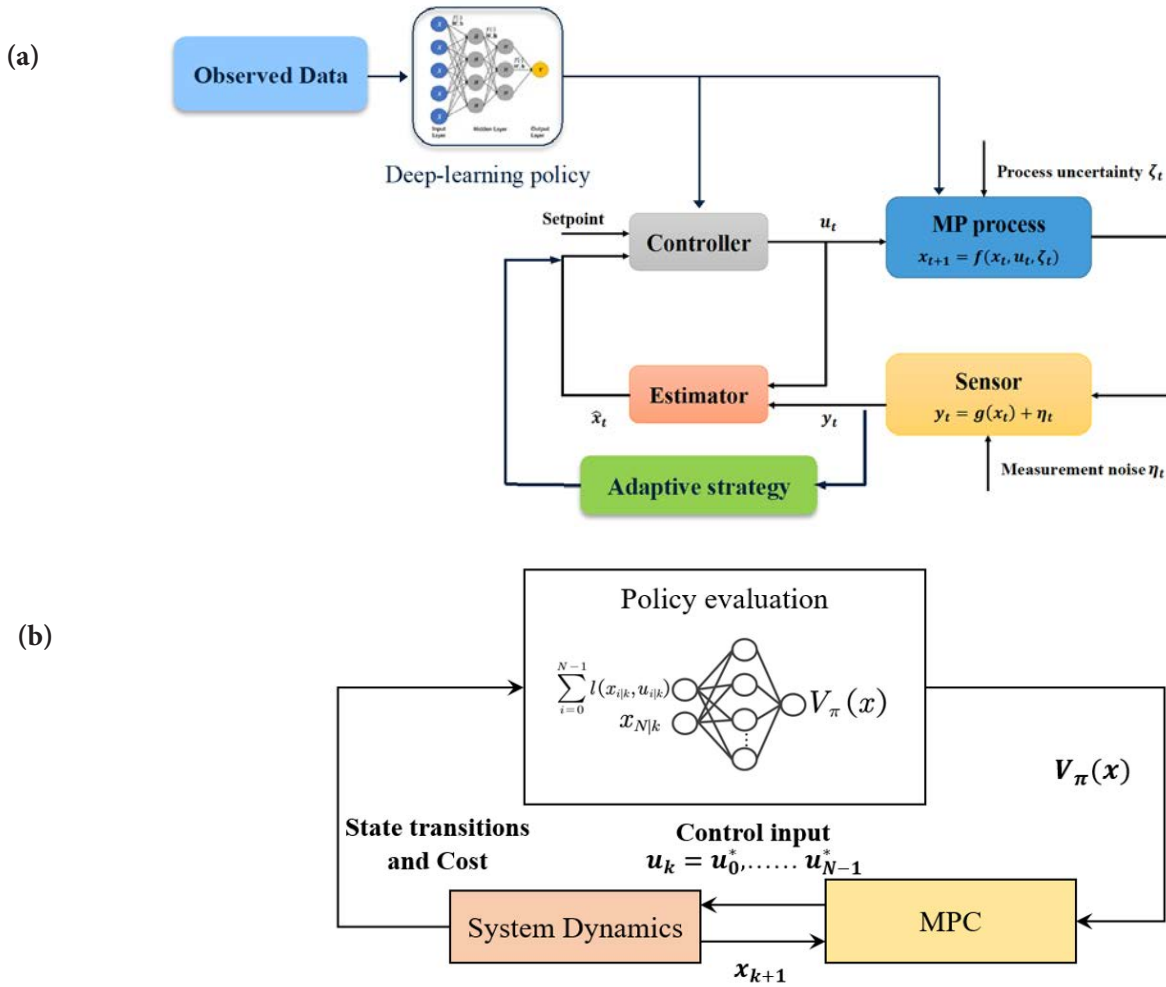


Figure 2. (a) RL-based MPC with a fixed policy. (b) RL-based MPC with variable policy

Proposed Methodology

In this methodology, the challenges with physics-based modeling and black-box modeling for predictive control are addressed by combining both these techniques. The dynamic behavior of the output variables and system disturbances are also captured. The order of auto-regression denoted by $\delta_{[y,w,u]}$ are hyperparameters chosen during cross-validation. In the learning step, y , w , and u time series were structured from raw sensor data to create data samples at each time instance. Deep neural networks are used for learning complex models with the adaptive updating laws for the weight parameters, as shown in Figure 2. The optimal control problem is defined as follows:

$$\text{minimize } u_0, \dots, u_{N-1} \sum_{t=0}^{N-1} W_i (y_{t+1} - y_{\text{ref}})^2 + u_t^T R u_t$$

$$\text{subject to } y_{t+1} = f(y_t, y_{t-1}, \dots, y_{t-\delta_y}, w_t, w_{t-1}, \dots, w_{t-\delta_w}, u_t, u_{t-1}, \dots, u_{t-\delta_u}), u_t \in \mathcal{U} \\ \forall t \in \{0, \dots, N-1\}$$

$$\hat{W}_i = P_i [\varphi_i(y_i)^T + \varphi_{i_f}^T e_{i_f} + k_i H_{i_f} \tilde{W}_i]$$

where u is the control input, w represents disturbances, N is the control horizon, R is the cost matrix, $W_i \in \mathbb{R}^{n_i \times n_i}$ is the weight matrix with n_i nodes, y_{ref} is the reference to be tracked, k_i is the convergence rate gain, e is the error, H_{i_f} is the admissible initial states, and P_i are the positive definite learning matrices.

PROJECT 1.2

Reinforcement Learning (RL) based Model Predictive Control (MPC) can be extended to incorporate both fixed and variable policies, offering flexibility in control strategies. In this hybrid approach, a fixed policy provides a baseline control, which can be a rule-based or handcrafted policy that offers stability and reliability. The variable policy, on the other hand, is learned and adjusted through RL, allowing the system to adapt to changing environmental conditions. The control action (u) is determined by a weighted combination of these policies, where α is the weight parameter:

$$u = \alpha \cdot u_{\text{fixed}} + (1 - \alpha) \cdot u_{\text{variable}}$$

Here, α can vary between 0 and 1, allowing the system to smoothly transition between the fixed and variable policies. The weight can be adjusted based on system confidence in the variable policy's performance. When $\alpha = 0$, the system relies entirely on the fixed policy, ensuring stability, while $\alpha = 1$ hands over control to the variable policy, enabling adaptation to changing conditions.

The variable policy, learned through RL, aims to optimize a certain objective function, typically a cumulative reward while satisfying system constraints. The policy is represented as a mapping from states (s) to control actions (u). Reinforcement learning algorithms, such as deep Q-networks (DQN) or proximal policy optimization (PPO), are used to update this policy iteratively based on the observed rewards and penalties. The variable policy seeks to improve control performance over time by learning from experience and adapting its behavior in response to system dynamics and environmental changes. This combination of fixed and variable policies allows for a high degree of control flexibility and adaptability, making it suitable for systems with varying operating conditions.

Preliminary Results

The proposed adaptive deep-learning-based MPC is developed for the high-consistency TMP process to demonstrate the energy cost reduction compared to the existing methods while ensuring closed-loop stability and convergence. It is assumed that all the variables in the MP process are measurable. In Figure 3 (a), the tracking performance has been achieved adequately for primary consistency. For the secondary consistency, a constraint has been imposed at 50%, and from Figure 3 (a), it is clear that the proposed method could satisfy the constraints and still track the setpoint. Figure 3 (b) compares the energy savings using the deep-learning MPC with the standard MPC.

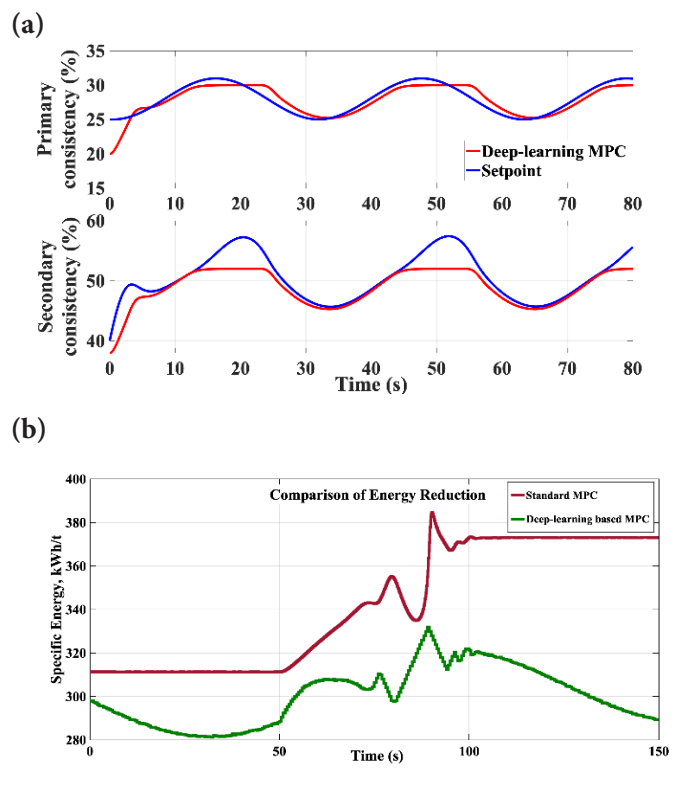


Figure 3. (a) State variables of the TMP process by using deep-learning MPC (b) Comparison of energy reductions.

Conclusions and Future Work

A deep-learning-based adaptive MPC has been developed, and some preliminary experiments have been performed on the high-consistency TMP process.

As a forward-looking endeavor in the paper and pulp industry, implementing predictive maintenance based on advanced data analysis holds immense potential. Leveraging historical data from sensors, machinery, and the manufacturing process, predictive maintenance can be developed to anticipate equipment failures and maintenance needs, reducing unplanned downtime and improving operational efficiency. By harnessing machine learning and data analytics, patterns of equipment degradation and failure modes can be identified, allowing for the timely scheduling of maintenance activities. This not only extends the lifespan of critical machinery but also optimizes resource allocation. With predictive maintenance, the paper and pulp industry can transition towards a proactive maintenance approach, ensuring uninterrupted production, lowering maintenance costs, and supporting the industry's sustainability efforts by minimizing waste and energy consumption.

CREATING LOW-ENERGY SHIVE-FREE PULPS

Authors: Rodger Beatson, Heather Trajano, Gloria Noki, Claire Maulit, Renz Po, Runxin Lai

Background

The objectives of this project are to: (1) understand the impact chemical treatments have on the development of fibre and fines' properties during LC refining, and (2) develop economically viable low energy processes that combine such treatments with LC refining to produce printing/writing, board and packaging grades.

Previous work by Chang et al. (2016) compared the effects of alkaline peroxide, chlorine dioxide, and ozone treatments with subsequent LC refining on TMP. Results showed that introducing oxidative agents reduces electrical energy consumption and improves pulp strength. Alkaline peroxide is hypothesized to generate acid groups on the surface of fibres and fines, increasing surface charge and causing surface fibre swelling. Swelling increases the bonded surface area and causes sheet densification. Chlorine dioxide and ozone oxidize lignin to produce carboxylic acids. A subsequent alkali soak forms sodium salt, which brings about softening and swelling of fibres and fines, leading to increase in tensile strength.

The current approach to optimize these technologies includes studying the kinetics of strength development during highly alkaline peroxide treatment (HAPT), and determining the contribution of fines to the property development of handsheets.

The rate of increase in tensile strength during HAPT is assumed to be dependent on temperature, the concentration of hydroxide ion (pH) and concentration of hydrogen peroxide. To provide a basis for the kinetic studies, we have determined how these chemical concentrations change during HAPT. Furthermore, as strength development is linked to acid group generation, we have investigated the kinetics of acid group development in the fibre and fines.

Materials and Methods

Highly Alkaline Peroxide Treatment

The secondary refiner TMP used in the HAPT study was provided by Holmen Braviken. The TMP was chelated with 0.2% or 0.6% charge diethylene triamine pentaacetic acid (DTPA) at 4% consistency in a 60°C water bath for 30 minutes. The pulp was then washed with deionized (DI) water with recirculation of filtrate to retain fines.

The chelated pulp was treated in plastic bags at 20% consistency with chemical charges based on the oven dried (OD) weight of pulp. HAPT was conducted with 6% sodium hydroxide (NaOH) and 3% sodium silicate (Na₂SiO₃) at 65°C for up to 120 minutes at either 2% or 6% peroxide (H₂O₂) charge, as shown in Figure 1. The pulp was mixed with the chemical solution by squeezing the bag. After treatment, the pulp was washed as described above.

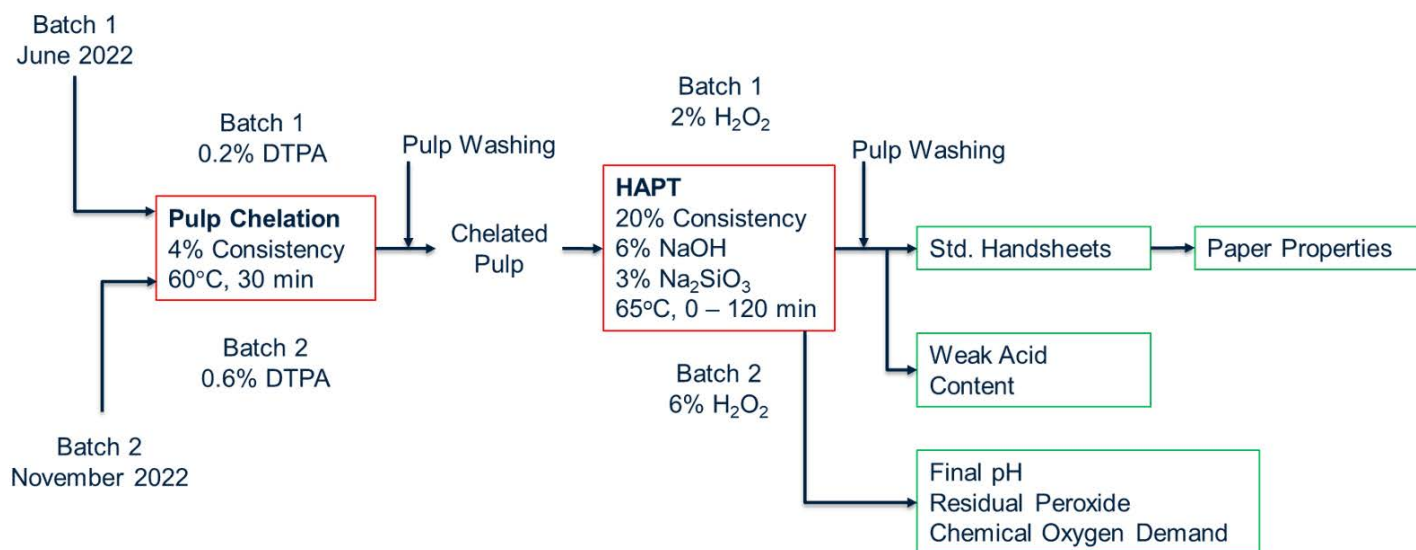


Figure 1. Experimental sequence used to study the kinetics of strength development in HAPT.

PROJECT 1.3

Characterization of HAPT Filtrate and Pulp

The final pH and chemical oxygen demand (COD) were measured from the filtrate collected after HAPT. The models we used to correlate COD to pulp yield loss were developed by Mobius (2006) and Pan (2018), whereby:

$$\text{COD} \left(\frac{\text{kg}}{\text{ton of OD pulp}} \right) = 0.34 \times \text{TOC} \left(\frac{\text{kg}}{\text{ton of OD pulp}} \right)$$

$$\text{TOC} \left(\frac{\text{kg}}{\text{ton of OD pulp}} \right) = 4.4173 \times \delta [\%] + 9.3454$$

where δ = Pulp yield loss.

Residual peroxide in the filtrate was measured using iodometric titration with 0.1 N sodium thiosulfate as the titrant.

Weak acid content of treated pulp was determined using conductometric titration (June 2022 Newsletter). Handsheets were prepared and tested according to TAPPI standard methods.

Kinetics of acid group generation in fibres and fines

The secondary refiner TMP used in the study of acid group generation in fibres and fines was provided by Alberta Newsprint Company. The HAPT protocol was as described above. The overall process is outlined below in Figure 2.

Separation of Fibers and Fines

20g OD pulp was hot disintegrated using standard procedures. DI water was added to achieve 0.5% consistency. The suspension was then placed in a 200-mesh sieve, and flushed with 16L of DI water. A Sommerville Shive agitator provided constant agitation, which prevented cake formation. Long fibres were collected in the sieve whereas the filtrate containing fines was collected in a bucket. After settling the filtrate overnight, it was dewatered by syphoning to recover fines.

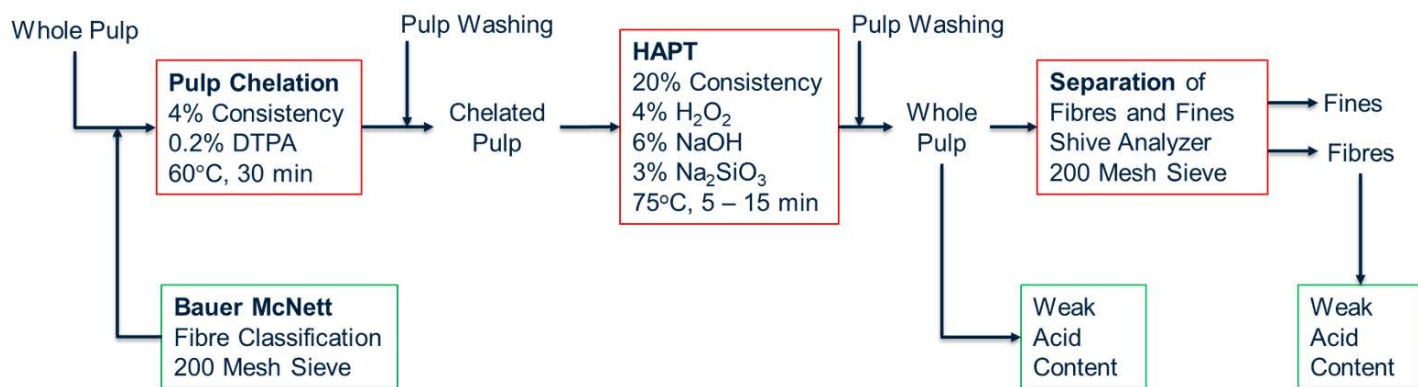


Figure 2. The experimental sequence used to study kinetics of acid group generation in fibres and fines.

Results

Figure 3 shows that tensile gains are rapid within the first 20 minutes of HAPT. Figure 4 shows that tensile strength increases linearly with increasing burst. This is due to the handsheet's isotropic nature. Figure 5 shows that tensile strength decreases with increasing bulk, which is consistent with decreased bonded area.

Figure 6(a) shows that tensile strength decreases with increasing opacity, which is consistent with decreased bonded area. The opacity is also dependent on absorption coefficient. As absorption coefficient increases the opacity will increase, as shown in Figure 6(b).

Figure 7 shows that the tensile strength decreases with increasing scattering coefficient, which is consistent with decreased bonded area.

Figure 8 shows that the initial brightness gain occurs before the strength gain. After which, the tensile strength increases at a rate of 1.6 Nm/g for every 1% ISO increase. In the June 2023 newsletter, we reported that if strength gain is the only priority, then 2% H₂O₂ is as effective as 6% H₂O₂; however, if good brightness and strength development are simultaneously desired, then a high charge of H₂O₂ is crucial.

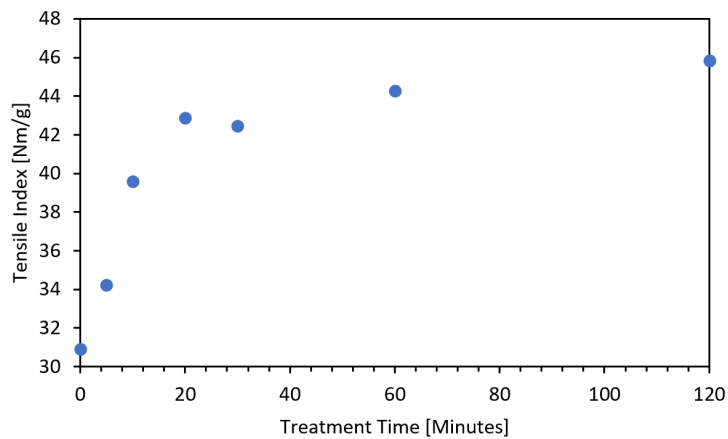


Figure 3. Tensile index over time for 6% H₂O₂ HAPT at 65°C.

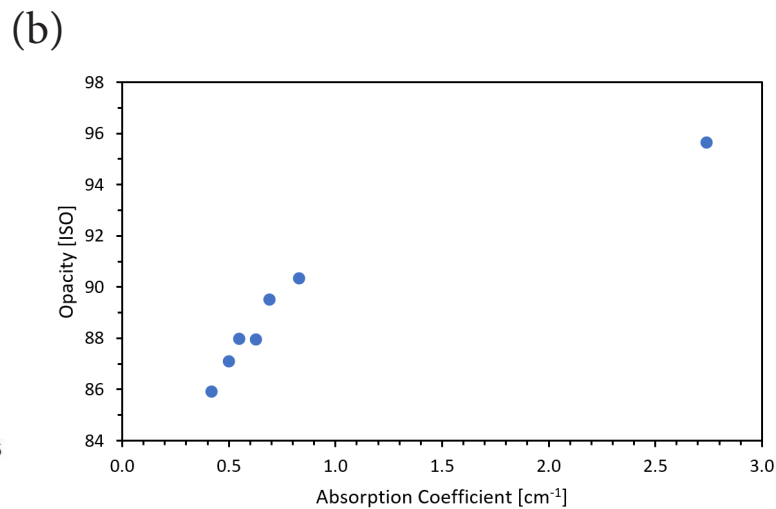
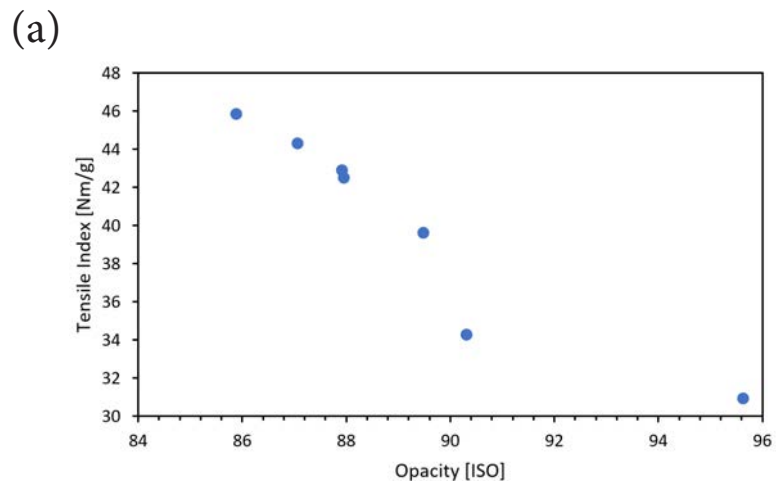


Figure 6. (a) Tensile index versus opacity for 6% H₂O₂ HAPT at 65°C. (b) Opacity versus Absorption Coefficient for 6% H₂O₂ HAPT at 65°C.

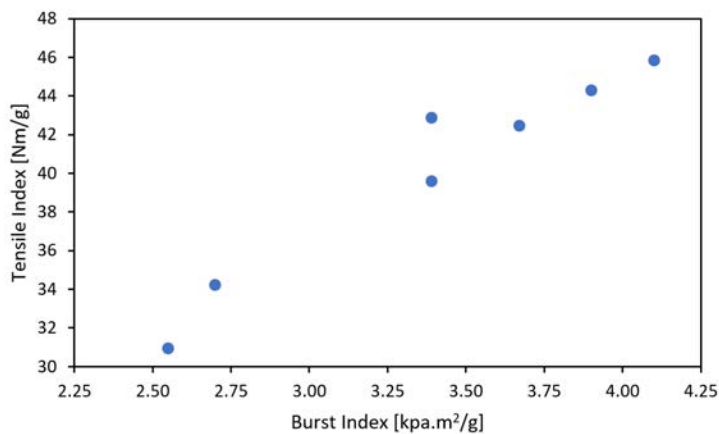


Figure 4. Tensile index versus burst index for 6% H₂O₂ HAPT at 65°C.

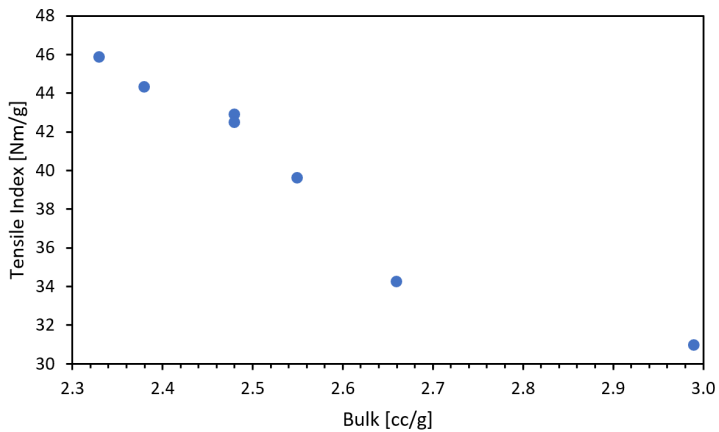


Figure 5. Tensile index versus bulk index for 6% H₂O₂ HAPT at 65°C.

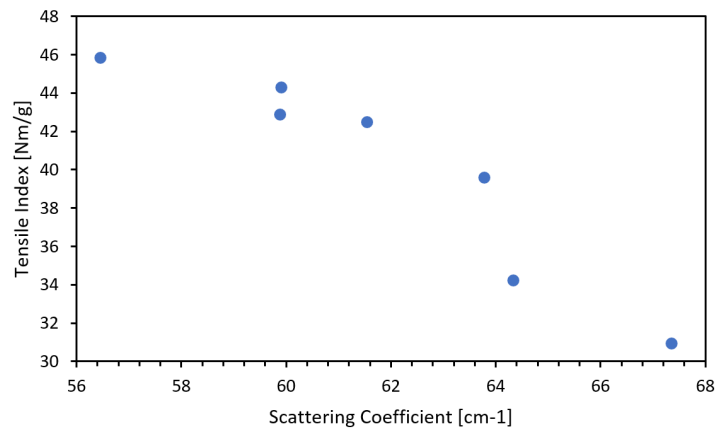


Figure 7. Tensile index versus scattering coefficient for 6% H₂O₂ HAPT at 65°C.

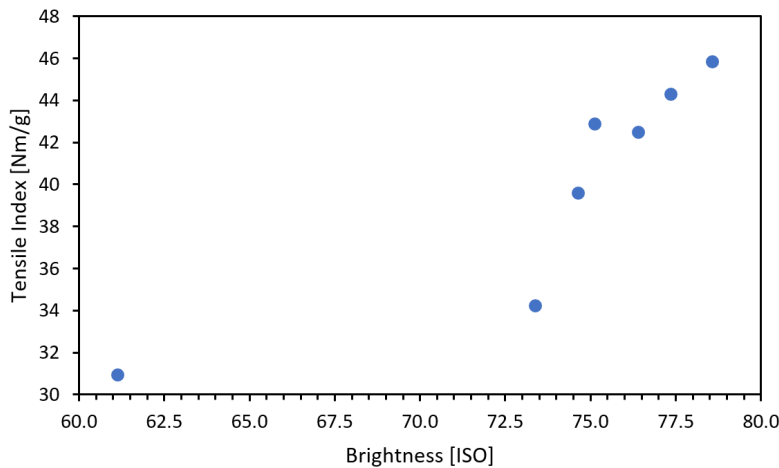


Figure 8. Tensile index versus brightness for 6% H₂O₂ HAPT at 65°C.

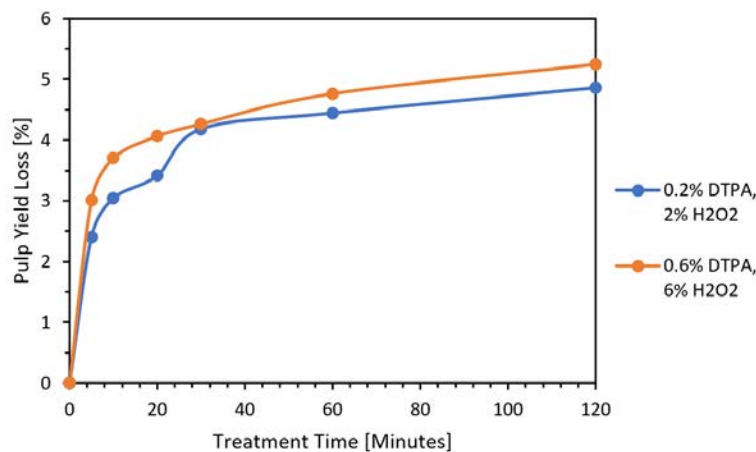


Figure 9. Pulp yield loss over treatment time.

Results (cont.)

Figure 9 shows that pulp yield loss, calculated from COD, increases rapidly then plateaus at around 4.5%. Pulp yield loss is similar for both the 2% and 6% peroxide charges. However, Figure 10 illustrates that the pH with 2% peroxide is greater than when 6% peroxide is used. Taken together, Figures 9 and 10 demonstrate that yield loss does not depend solely on pH.

Acid Group Generation in Fibres and Fines

To determine the effect of fines on strength development, non-treated (control) or HAPT-treated fines were added with non-treated fibre suspensions prior to handsheet formation. Figure 11 shows that tensile index of the tested handsheets increased more rapidly with increasing HAPT fines.

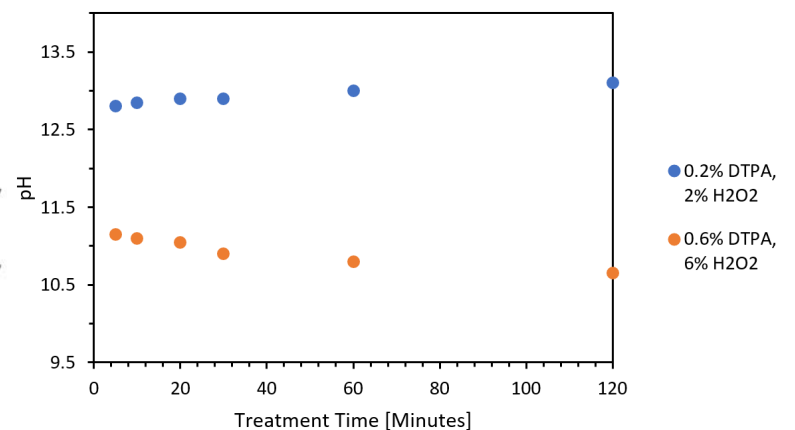


Figure 10. pH over treatment time.

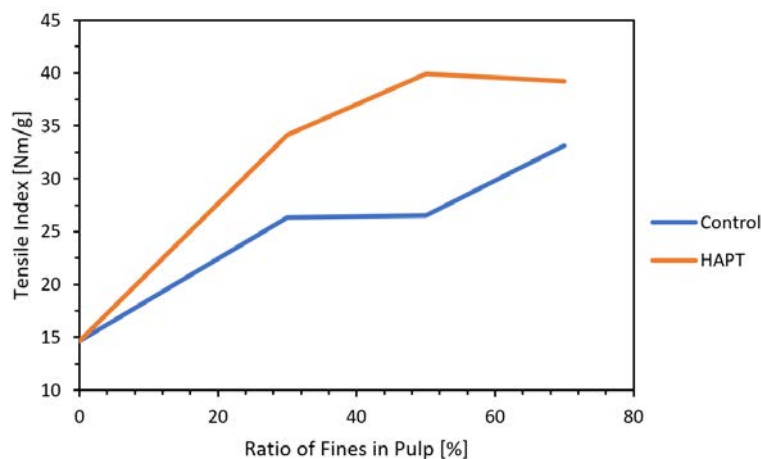


Figure 11. Tensile index vs fines ratio added to nontreated fibres. The HAPT fines were generated by treating whole pulp at 20% consistency with 6% sodium hydroxide (NaOH), 3% sodium silicate (Na₂SiO₃), and 4% hydrogen peroxide at 75°C for 120 minutes. After treatment, fines were separated from long fibres as described above.

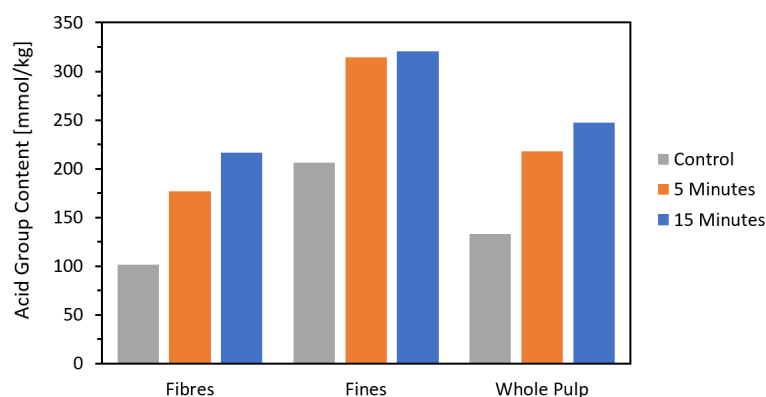


Figure 12. Acid group content of fibres, fines and whole pulp. Pulp received from Alberta Newsprint. The HAPT treated fines were generated by treating whole pulp at 20% consistency with 6% sodium hydroxide, 3% sodium silicate, and 4% hydrogen peroxide at 75°C for up to 15 minutes. After treatment, fines were separated from long fibres as described above.

The acid group content of isolated fibres and whole pulp was measured directly by titration. The acid group content of fines was then calculated by mass balance. Figure 12 shows acid group content for untreated pulp (control) and HAPT materials. During HAPT, acid group generation occurs much more rapidly in the fines, reaching over 300 mmol/kg pulp within 5 minutes of treatment. After 5 minutes, further acid generation primarily occurs in the fibres. We hypothesize that this difference is due to the small size and large surface area of fines.

The rate of acid group generation may be diffusion limited; that is, acid groups are first preferentially generated on fines as well as external fibre surfaces and then within fibre walls.

Conclusions

Tensile strength increases rapidly during the first 20 minutes of HAPT. The alkaline peroxide reaction occurs the same time scale as tensile strength development; that is, rapidly and primarily with fines during the initial stages of the reaction. The increase in tensile index of handsheets with increased HAPT fines indicates that hydrogen peroxide reacts with the fines to promote rapid development of tensile strength. Additionally, the reduced scattering coefficient and opacity indicate that the strength gains result from increased bonded area. Therefore, further supporting the correlation exists between the kinetics of strength development and the kinetics of acid group generation in fibres and fines.

Future Work

In future work, a detailed characterization of fines and fibres prior to and post HAPT will be performed. We will continue our investigation of the hypothesis that tensile strength development results from acid group generation on fines and external fibre surfaces.

References

1. Beatson, R., Trajano, H., Mitra, S., K., and Maulit, C. (2021, November). ERMP November 2021 Newsletter. Energy Reduction in Mechanical Pulping. https://ermp.sites.olt.ubc.ca/files/2022/06/ERMP_Nov2021.pdf
2. Chang, X. F., Luukkonen, A., Olson, J., & Beatson, R. (2016). Pilot-scale investigation into the effects of alkaline peroxide pre-treatments on low-consistency refining of primary refined softwood TMP. *Bioresources*, 11(1), 2030-2042. <https://doi.org/10.15376/biores.11.1.2030-2042>
3. Cheng, X. F., Olson, J. A., & Beatson, R. P. (2011). A comparison between the effects of ozone and alkaline peroxide treatments on TMP properties and subsequent low consistency refining. *Bioresources*, 7(1), 99-111. <https://doi.org/10.15376/biores.7.1.99-111>
4. Dence, C., W., and Omori, S., (1996). Survey of hydrogen peroxide bleaching of mechanical and (chemi)mechanical pulp - factors affecting brightness. *Pulp Bleaching: Principles and Practice: TAPPI 1996*, pp. 457-489.
5. Engstrand, P., Sjogren, B., Olander, K., and Htun, M., (1991). The significance of carboxylic groups for the physical properties of mechanical pulp fibres. 6th International Symposium Wood Pulping Chemistry, pp. 75-79.
6. Maulit, C., Beatson, R., Trajano, H., Po, R., and Lai, R. (2022, November). ERMP November 2022 Newsletter. Energy Reduction in Mechanical Pulping.
7. Mitra, S., K., Maulit, C., Beatson, R., and Trajano, H. (2022, June). ERMP June 2022 Newsletter. Energy Reduction in Mechanical Pulping. https://ermp.sites.olt.ubc.ca/files/2023/01/ERMP_June2022.pdf
8. Moldenius, S., (1984). The Effects of Peroxide Bleaching on the Strength and Surface Properties of Mechanical Pulping. *Journal of Pulp and Paper Science.*, vol. 10, pp. 172-177.
9. Mobius, C. H. (2006). *Water Use and Wastewater Treatment in Papermills*. Augsburg, Germany: Herstellung und Verlag
10. Noki, G., Beatson, R., Trajano, H., Maulit, C., Po, R., and Lai, R. (2023, June). ERMP June 2023 Newsletter. Energy Reduction in Mechanical Pulping.
11. Pan, H. Y. G. (Accessed February 2018). Measurement of dissolved organic substances as a predictive tool to monitor pulp qualities in the alkaline peroxide bleaching of aspen mechanical pulp. *Pulp and Paper Canada*.

PROJECT 2.1

LIGNIN RICH FINES: SIMPLE ROUTES TOWARDS CREATION OF HYDROPHOBIC AND HYDROPHILIC FILLER ADDITIVES

Authors: Adam Wu, Siwei Chen, and Scott Rennecker

Fines as PLA filler additives

Previously, we reported on surface modification through esterification using anhydride compounds, which increased the hydrophobicity of fines to enhance dispersion in a PLA matrix. We also detailed mechanical treatment via ball milling of fines, an alternative approach that proved efficient for evenly distributing fines within the PLA matrix. Based on a number of mechanical tests, this latter route resulted in the most optimal performance among all PLA/fine composites. Furthermore, we have successfully demonstrated 3D printing using filament that contains 10% ball-milled (Bm) fines. To further enhance the interface between the fines dispersed in the PLA matrix and improve the mechanical properties of the composites, we applied coupling agents in the melt. The coupling agents were expected to function as a bridge between wood materials and the polymer matrix by inducing chemical reactions during blending with fillers to entangle with the matrix, thereby providing direct interaction between the components and enhancing interfacial adhesion (Huda et al. 2006; Chauhan et al. 2021).

In this research, both maleic anhydride-grafted polypropylene (MAPP) and maleic anhydride-grafted PLA (MAPLA) were utilized to facilitate intimate bonding between fines and PLA. These two coupling agents bear similarity to the anhydride compounds used in our previous chemical modifications of

fines. The succinic group in maleic anhydride can react with the hydroxyl groups on the surface of the fines, forming ester linkages and carboxylic acids, which creates robust bonding between fines and PLA. To explore the impacts of adding coupling agents to PLA/fine composites, we melt-compounded PLA with 10% TMP fines and 10% Bm fines, both with and without coupling agents, and conducted tensile tests and rheological tests on them.

Results

The tensile test results were assessed using a one-way ANOVA test to determine any statistically significant differences among all composites. In Figure 1, values marked with different letters are considerably different at an α level of 0.05. It was found that the introduction of coupling agents did not yield a notable enhancement in terms of tensile strength and modulus. The inclusion of MAPP resulted in a reduction of both properties as shown in Figure 1 (a). On the other hand, a contrasting trend for elongation at break and toughness was observed with MAPP (Figure 1 (b)). Specifically, the addition of MAPP led to a significant increase in elongation at break (by 107% and 59%) and toughness (by 117% and 55%) for PLA/Bm fines and PLA/TMP fines composites, respectively. However, this toughening effect was nonsignificant for MAPLA coupling agents.

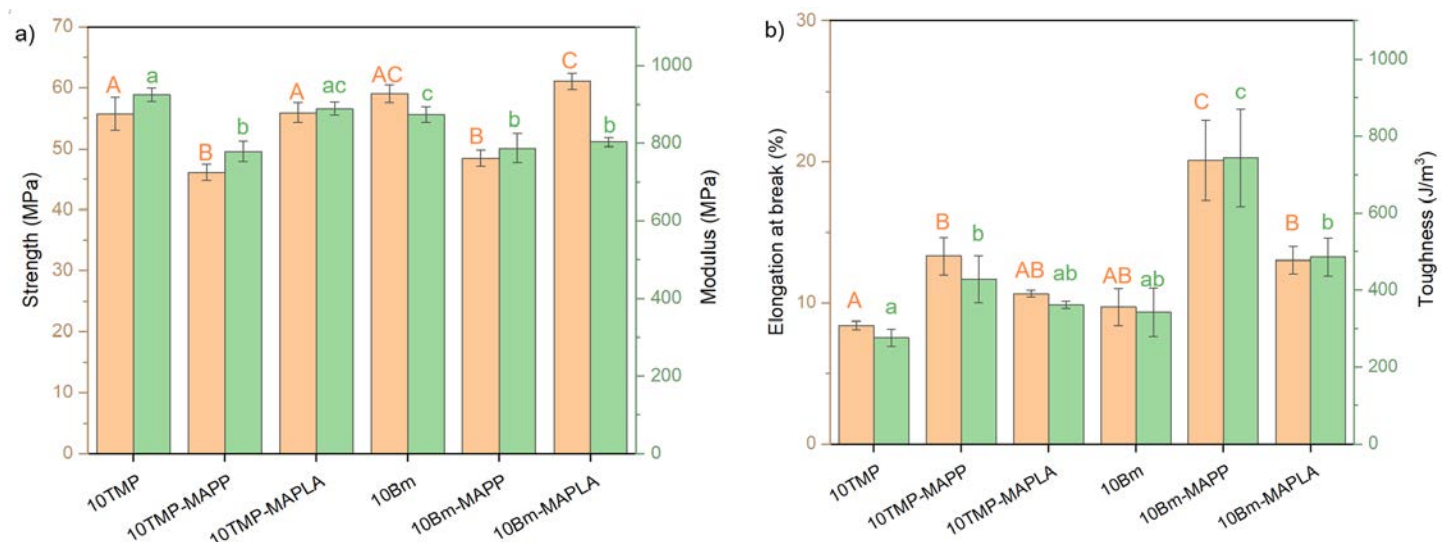


Figure 1. a) Tensile modulus and tensile strength, b) Elongation at break and toughness of PLA and PLA/fine Composites

PROJECT 2.1

Following this analysis, we used scanning electron microscopy (SEM) to investigate the interphase interactions by evaluating the fracture surfaces of the composites. Figure 2 presents representative images of fractured surfaces of PLA/TMP fines as well as PLA/Bm fines both with and without MAPP or MAPLA. In PLA/TMP fines, no coupling agent and with MAPP (Fig 2a-b) both exhibited rough surfaces and fine aggregates. Although the tensile properties were not improved with the addition of MAPLA, it seemed to facilitate the distribution of TMP

fines within the PLA. The fracture surface shown in Figure 2c exhibited reduced phase separation caused by fine aggregates, suggesting an interaction between the ball-milled fines and PLA (Fig 2d). Concerning the ball-milled fine samples (Fig 2d-f), the one containing MAPP presented a stretched fracture surface, indicating higher ductility. This characteristic also explains the observed increase in elongation at break and toughness. The introduction of MAPLA did not result in significant changes to the PLA/Bm fines.

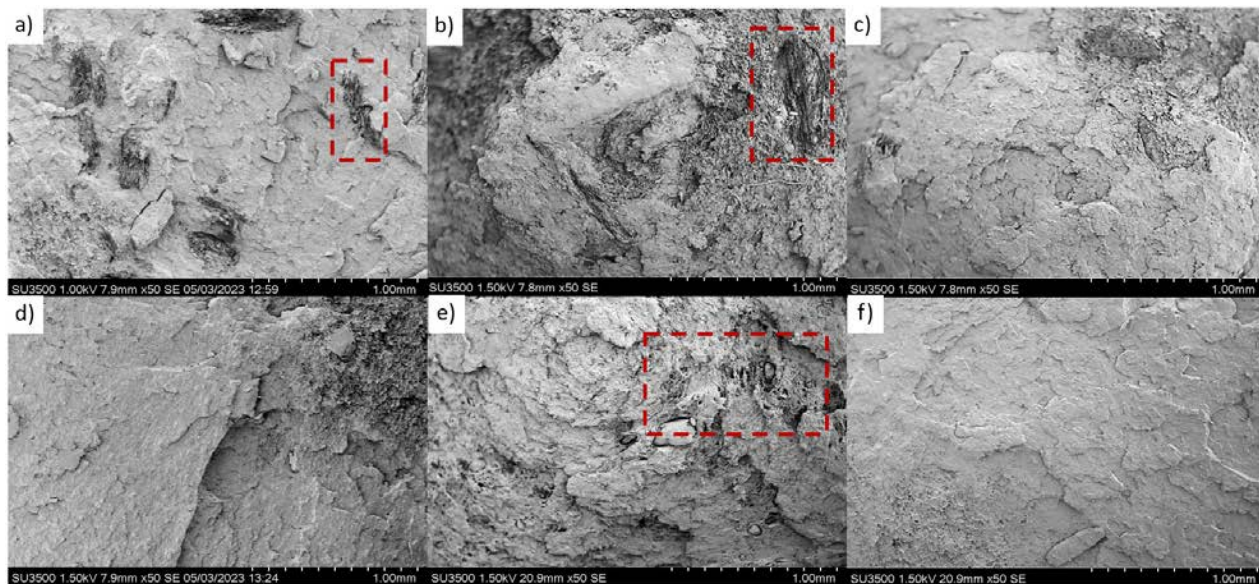


Figure 2. SEM images of PLA composites with a) TMP fines, with b) TMP fines and MAPP, c) TMP fines and d) MAPLA, e) Bm fines and MAPP, f) Bm fines and MAPLA

To predict the printing process and the quality of the final product, a thorough understanding of the rheological properties is necessary, as these properties significantly impact the material's behaviour during the 3D printing process. For instance, viscosity reflects the flowability and extrudability of the melt through the nozzle of the 3D printer, as well as the shape stability after extrusion. Elasticity determines the material's response to changing stress and strain during printing (Herrada-Manchón et al. 2023).

In an investigation into the viscoelastic characteristics, oscillatory rheological tests were employed to assess the complex viscosity and dynamic moduli of the composites. As Figure 3 shows, pure PLA displayed a Newtonian plateau in the low-frequency range, coupled with mild shear thinning behaviour (lower viscosity at higher shear rates). Upon the introduction of fines, the behaviour transitioned to non-Newtonian, accompanied by yield stress in the low-frequency region, and the complex viscosity at high frequencies was found to be lower than that of pure PLA. This introduction of fines also resulted in more pronounced shear

thinning behavior compared to pure PLA, which was revealed to enhance the processability of polymers in the printing process (Compton and Lewis 2014; Bertolino et al. 2021). Because a pronounced shear thinning property indicated that the viscosity of the material is low enough to allow extrusion from the nozzle, yet high enough upon exiting to prevent dripping. Beyond that finding, adding coupling agents diminished the viscosity at high frequencies even further suggesting that the interaction among PLA molecules was disturbed by the inconsistently dispersed additives (Bertolino et al. 2021). For the effective bonding of the printed part, it is preferable that the storage modulus be lower than the loss modulus ($G' < G''$). This condition suggests a complete relaxation and diffusion of extruded polymer chains, which facilitates the welding of consecutively deposited layers by the 3D printer (Yang et al. 2021). An exception is TMP fines with MAPP sample, which demonstrated a shift towards solid-like behaviour ($G' \geq G''$) in the low to intermediate frequency region, while all other samples exhibited viscous behaviour ($G' \geq G''$) in the terminal region.

PROJECT 2.1

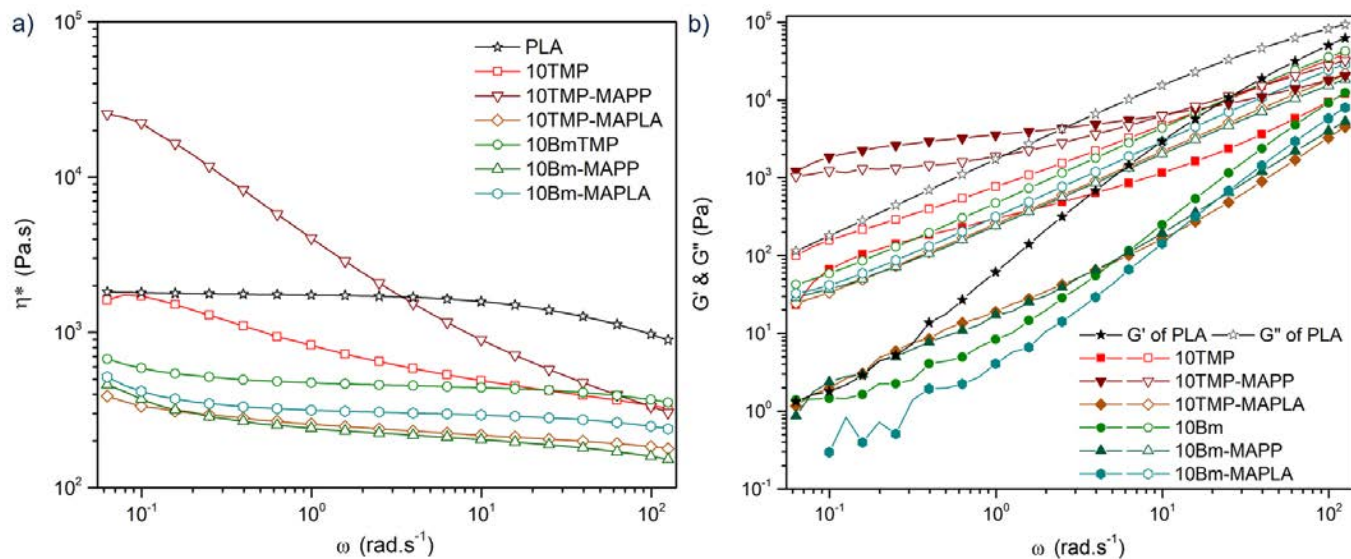


Figure 3. a) Viscosity and b) Dynamic moduli as a function of frequency for PLA/fine composites

In conclusion, this study identified and compared the effects of adding two coupling agents to enhance the interfacial adhesion between fines and polylactic acid (PLA). It was demonstrated that the integration of maleic anhydride grafted polypropylene (MAPP) with PLA/fine composites increases the elongation at break and toughness of the composites. However, this increase was accompanied by a reduction in both tensile strength and modulus. The addition of MAPP to fine-based PLA composites facilitated the even dispersion of fines, but it did not enhance the mechanical properties. The viscosity of all PLA/fine composites at high frequencies was lower than that of pure PLA, ensuring the likely flowability of the composites through the 3D printer nozzle. While the TMP-MAPP sample exhibited a marked elastic behaviour, it might experience incomplete relaxation after printing. The remaining samples are expected to ensure adequate interlayer bonding for the printed parts.

Future work

In future studies, to determine the viscosity of materials under conditions that more closely simulate those in 3D printing, we intend to conduct steady-shear rheology tests. Additionally, we plan to select the most and least promising candidates for filament production and subsequently test them in a 3D printer to validate the rheological findings. Concerning the mechanical treatment of fines, we are considering the combination of never-dried fines with PLA in a Brabender mixer as an alternative to the freeze-drying and ball milling processes where moisture is driven off during compounding.

Fines as paper strength additives

Mechanical pulp fines can impact the mechanical properties of the resulting paper positively or negatively, making them potential additives for paper strength improvement. It is anticipated that modifying fines by increasing their hydrophilicity, to boost hydrogen bonding with pulp fibers, could enhance their effectiveness as dry-strength additive. Recent work (Beaumont et al. 2021) demonstrating the use of succinic anhydride and imidazole at mild reaction condition was followed to modify the primary C₆-OH groups of cellulose into carboxylic acid groups through regioselective surface esterification. We employed a similar reaction (40°C for 6.25 hours) on softwood mechanical pulp fines, with the hope of increasing their hydrophilicity and making them more suitable as additives for enhancing paper strength.

Results and discussion

The initial work focused on the characterization of the fines. As described in previous reports, the fines are highly heterogeneous, generally composed of fibrillar and flake-like fines. Chemical composition analysis of fines indicated that there was high concentration of lignin, which was in agreement with previous studies indicating fines contain more lignin (largely derived from cell corners) than the rest of the pulp (Fromm et al. 2003; Kangas and Kleen 2004). Laser diffraction analysis of fines using Mastersizer indicated that the particle size of fines falls within the range of 10 to 100 micrometers (Figure 4a).

PROJECT 2.1

Based on these analyses, it seems that the direct esterification of fines with succinic anhydride (SA) and imidazole (described as “SA-modified” in this paper) did not significantly influence the morphology of TMP fines. As anticipated, after SA modification, it was apparent that the fines contained more carboxylic acid groups (from 0.1 to 0.5 mmol g⁻¹) as determined using a conductric titration method (Figure 4b). The suspension of fines were also subjected to determination of zeta-potential in the deionized water, which confirm the enhanced negative charges of fines after SA modification, as a result of carboxylic acid groups incorporation and deprotonation (Figure 4b).

It was anticipated that the incorporation of carboxylic acid groups onto TMP fines could enhance their hydrophilicity, which is an important aspect of various paper strength additives (Hubbe 2006). In this work, the hydrophilicity of fines was estimated by dynamic vapor sorption (DVS) technique, which measured the weight change of substrates at different moisture content and provides adsorption and desorption curves during the dynamic

moisture sorption experiments. Comparing SA-modified fines with starting substrates, it was apparent that modified fines were more prone to absorbing moisture, as indicated by its more significant weight increase with increasing relative humidity (from 0 to 70%), and greater ability to retain moisture with reducing relative humidity (Figure 4c). In particular, at relative humidity of 70% which was set as the maximum value, the SA-modified fines were found to absorb 30% more moisture as compared to unmodified fines (Figure 4c). With the notion that the increased hydrophilicity of fines would result in stronger intermolecular bonding between individual particles, the unmodified and SA-modified fines were filtered and dried into films for stress-strain analysis. As anticipated the SA modification had significant influence on the bonding strength of the individual fines, with this approach leading to 179% and 159% increase in Young’s modulus and tensile strength of the resulting films, respectively (Figure 4d).

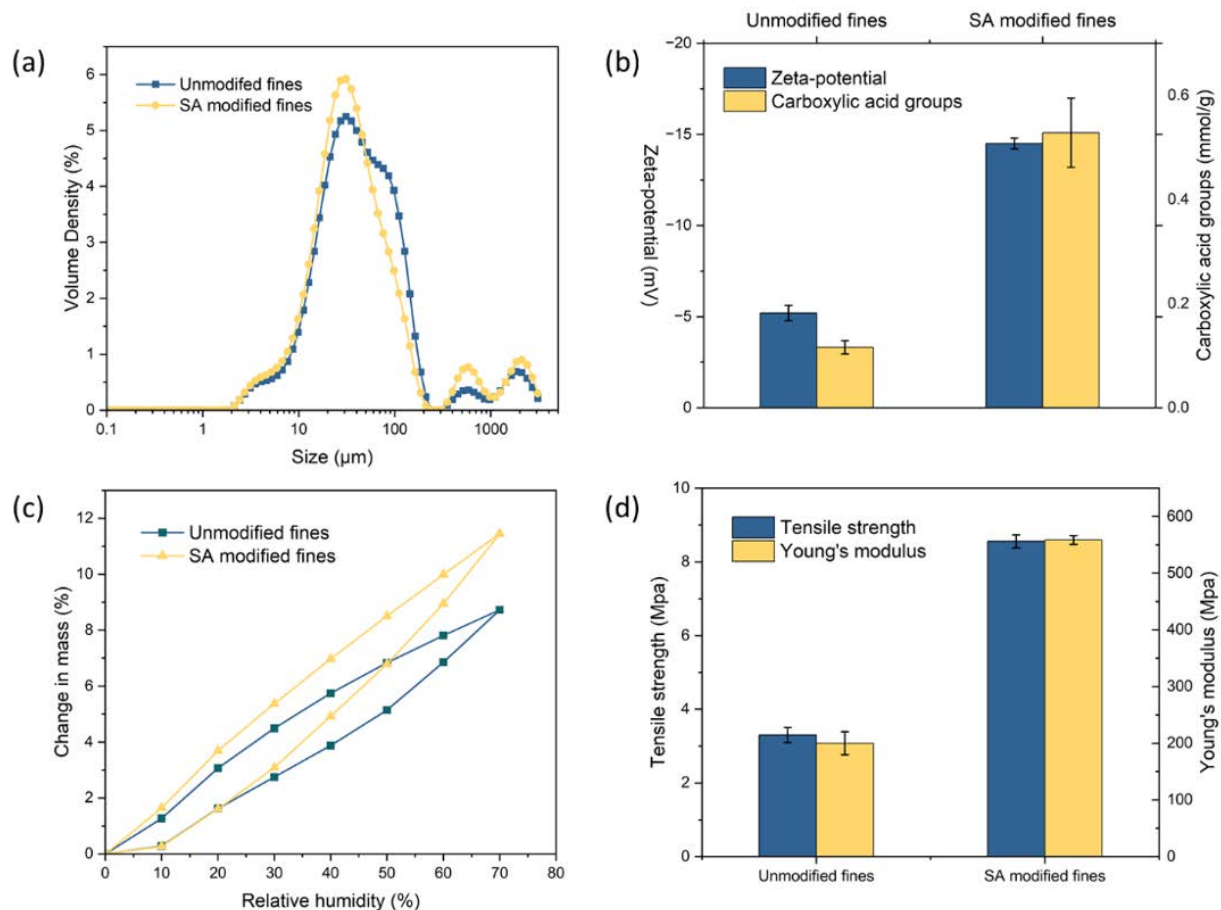


Figure 4. Characteristics of Unmodified and SA-Modified Fines: (a) size distribution of fines as measured by laser diffraction particle size analyzers, (b) Zeta-potential and carboxylic acid group content of fines, (c) fines’ capacity to absorb moisture as determined by dynamic vapor sorption (DVS) analysis, and (d) mechanical strength of films derived from unmodified and SA-modified fines.

PROJECT 2.1

After observing promising features in SA-modified TMP fines on their own, the next step of this project was to investigate the potential enhancement of pulp mechanical properties, using softwood TMP as the feedstock. This was carried out by substituting 10 wt.% of the pulp with the unmodified and SA-modified fines prior to the production of handsheets, which were subjected to measurement of tensile, burst and tear strengths, as typical paper strength characteristics. Although it was anticipated that the substitution of SA-modified fines could significantly improve the mechanical properties of the low quality TMP, there was only minor improvement (2-3%) in tensile strength after substitution of unmodified and SA-modified fines (Figure 5a), and a slight increase (16%) in burst index in the case of SA-modified fines (Figure 5b). In both cases the tear index of the resulting handsheets decreased by 12% (Figure 5c). The moderate effect of fines addition on the improvement of mechanical strength of handsheets can be attributed to the high content of fines in the pulp, as the TMP contained high content (43.5%) of fines (particles with a length between 0.07 and 0.2mm) as determined with a Fibre Quality Analyzer. It should be noted that the substitution of pulp with fines can only benefit the strength of paper to a certain extent (Odabas et al. 2016), and a high content of fines in the pulp mixture would offset the strength of the fiber network made by long fibers. In addition, it was reported that the maximum allowable fines content for improving the tear strength of paper was very low (Odabas et al. 2016). This low threshold could be the reason for the negative impact of fines addition on the tear strength of TMP-derived handsheets. Therefore, it appears that the presence of a high fines content in the original TMP pulp hinders the strength improvement from the substitution of SA-modified fines. To evaluate this notion, the subsequent work attempted to remove fines from the current

TMP pulp using the Bauer-McNett fiber classifier, which was capable of fractionating fibres according to the fibre length using the various screens (14-200 mesh). According to the Bauer-McNett classifier, the fines fraction (particles smaller than 200 mesh) contains around 20% of the entire pulp slurry by weight (which was slightly different than the result of FQA due to the different measuring mechanisms), and the majority of the fibers fell under the category of 28-48 mesh. To collect only the "fines-free" fraction, we then collected only the fibers that are larger than the 100-mesh fraction (i.e., 100, 48, 28, and 14) for the subsequent work.

As shown in Table 1, although we were only collecting fractions greater than 100 mesh which had an average arithmetic fiber length of 1.47 mm, it was still shown in the FQA that this fractionated pulp retained around 29% (by number) of fines, although this is much lower than that of the starting TMP (43.5%). When we substituted the fractionated TMP with unmodified and SA-modified fines, it was found that a 10% substitution of both fines resulted in around a 10% increase in the tensile index of the handsheets (Figure 6a) and a slight reduction in the burst index (Figure 6b) and tear index (Figure 6c). When we further increased the loading of fines to 20%, the selection of SA-modified fines resulted in a significant improvement in the tensile index of 30%, while the beneficial effect of unmodified fines remained close to 10% (Figure 6a). Additionally, 20% SA-modified fines substitution resulted in a 24% increase in burst index, whereas unmodified fines only resulted in a 7% increase (Figure 6b). It was also apparent that the addition of fines had the least negative impact on the tear index of the resulting TMP handsheets, as only a 20% SA-modified fine substitution led to a 3% increase, while all other attempts reduced the tear index by 3-7% (Figure 6c).

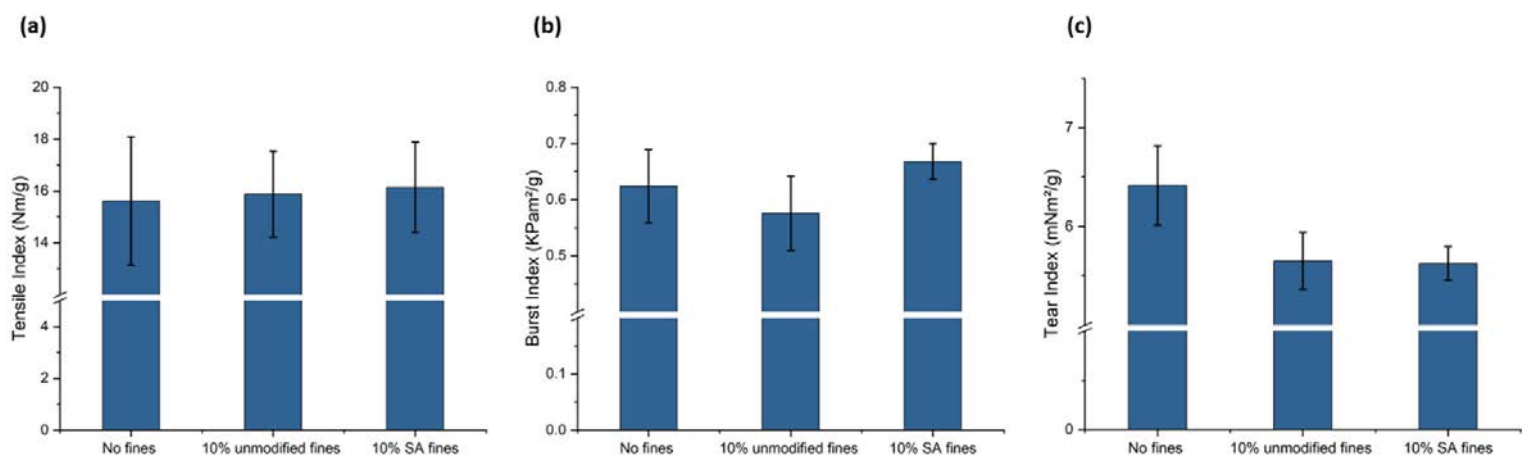


Figure 5. Tensile (a), burst (b) and tear (c) strength of handsheets made from starting thermomechanical pulp (TMP) with and without the addition of unmodified and SA-modified fines

Table 1. Length and fines content of fibers from starting thermomechanical pulp (TMP), fractionated TMP, and bleached chemi-thermomechanical pulp (BCTMP), as measured by FQA.

Sample	Mean length (0.2-10mm)		Mean % fines (0.07 mm–0.2mm)		Mean width (mm)
	Arithmetic (mm)	Length Weighted (mm)	Arithmetic (%)	Weighted (%)	
TMP before fibre classifier	1.14 (0.05)	1.86 (0.04)	43.5 (2.0)	7.3 (0.8)	31.3 (0.3)
TMP after fibre classifier	1.47 (0.03)	2.20 (0.05)	29.4 (0.9)	3.7 (0.2)	31.1 (0.4)
BCTMP	1.25 (0.03)	2.21 (0.04)	37.8 (2.3)	5.3 (0.7)	33.6 (0.6)

Future work

With the reported work indicating the successful esterification of fines using SA treatment, our future plans involve further fibrillating the SA-modified fines using a microfluidizer, with the hope of producing nano-fibrillated materials derived from fines that would give more potential for interactions with pulp surfaces within the handsheet.

Acknowledgements

We would like to thank our undergraduate research assistant, Nicole Ting, for her invaluable contribution to the experimental sessions.

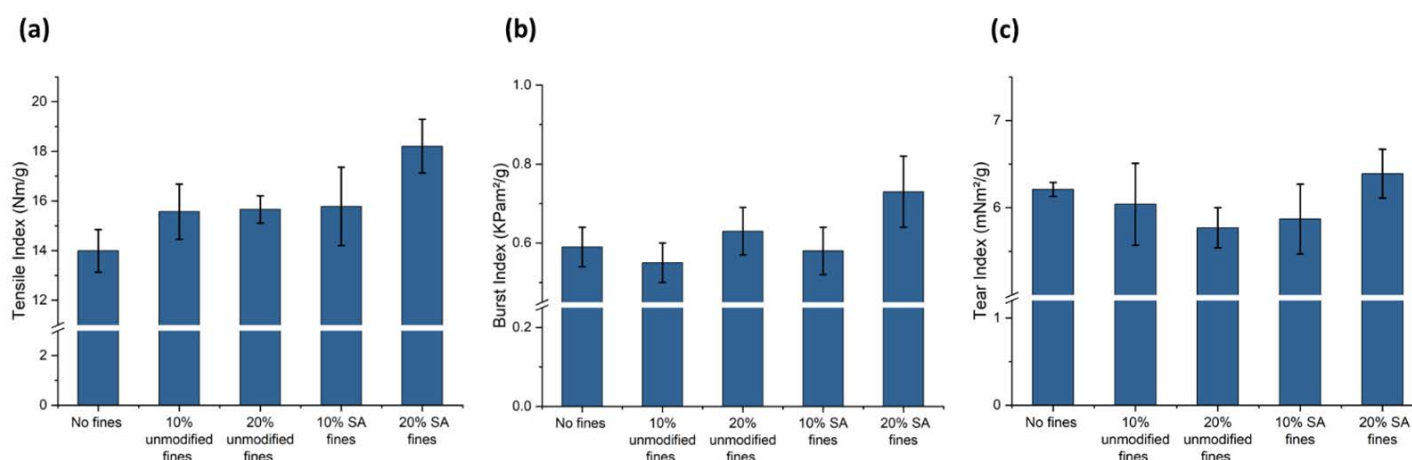
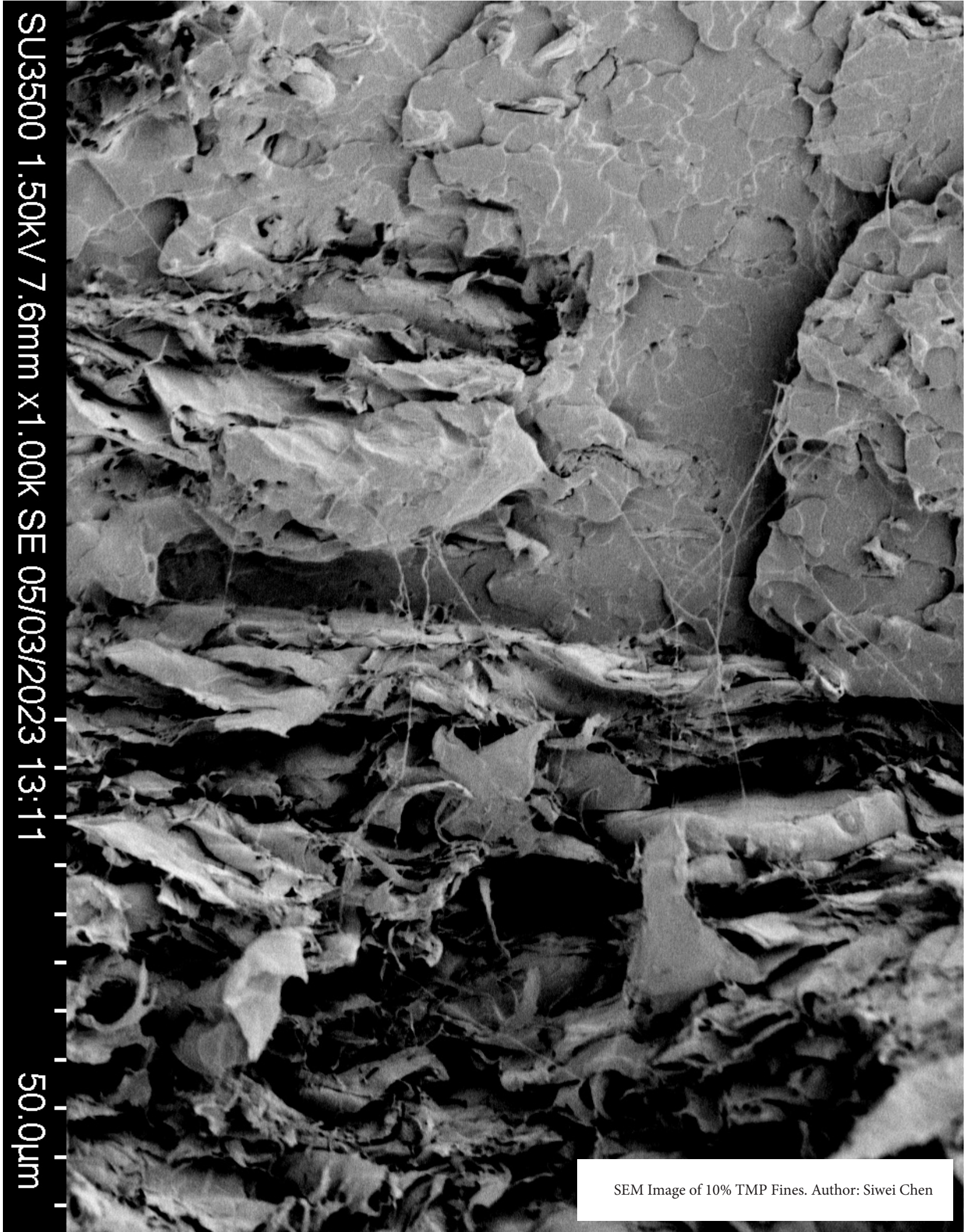


Figure 6. Tensile (a), burst (b) and tear (c) strength of handsheets made from the long fibres isolated from thermomechanical pulp (TMP) with and without the addition of unmodified and SA-modified fines.

References

1. Beaumont M, Tardy BL, Reyes G, et al (2021) Assembling Native Elementary Cellulose Nanofibrils via a Reversible and Regioselective Surface Functionalization. *J Am Chem Soc* 143:17040–17046.
2. Bertolino M, Battagazzore D, Arrigo R, Frache A (2021) Designing 3D printable polypropylene: Material and process optimisation through rheology. *Addit Manuf* 40:101944.
3. Chauhan S, Raghu N, Raj A (2021) Effect of maleic anhydride grafted polylactic acid concentration on mechanical and thermal properties of thermoplasticized starch filled polylactic acid blends. *Polym Polym Compos* 29:S400–S410.
4. Compton BG, Lewis JA (2014) 3D-printing of lightweight cellular composites. *Adv Mater* 26:5930–5935.
5. Fromm J, Rockel B, Lautner S, et al (2003) Lignin distribution in wood cell walls determined by TEM and backscattered SEM techniques. *J Struct Biol* 143:77–84.
6. Herrada-Manchón H, Fernández MA, Aguilar E (2023) Essential Guide to Hydrogel Rheology in Extrusion 3D Printing: How to Measure It and Why It Matters? *Gels* 9:.
7. Hubbe M (2006) Bonding between cellulosic fibers in the absence and presence of dry-strength agents – A review. *BioResources* 1:281–318.
8. Huda MS, Drzal LT, Misra M, Mohanty AK (2006) Wood-fiber-reinforced poly(lactic acid) composites: Evaluation of the physicomechanical and morphological properties. *J Appl Polym Sci* 102:4856–4869.
9. Kangas H, Kleen M (2004) Surface chemical and morphological properties of mechanical pulp fines. *Nord Pulp Pap Res J* 19:191–199.
10. Odabas N, Henniges U, Pothast A, Rosenau T (2016) Cellulosic fines: Properties and effects. *Prog Mater Sci* 83:574–594.
11. Pettersson G, Norgren S, Engstrand P, et al (2021) Aspects on bond strength in sheet structures from TMP and CTMP – A review. *Nord Pulp Pap Res J* 36:177–213.
12. Yang Z, Feng X, Xu M, Rodrigue D (2021) Printability and Properties of 3D-printed Poplar Fiber/Polylactic Acid Biocomposite.



SU3500 1.50kV 7.6mm x1.00k SE 05/03/2023 13:11

50.0µm

SEM Image of 10% TMP Fines. Author: Siwei Chen

FROM TREES TO TREATMENT: FUNCTIONALIZING TMP EXTRACTIVES

Authors: Cameron Zheng, Henok Sahile, Brent Page, Laurel Schafer, Heather Trajano

Background

Extractives such as terpenes are used as natural medicines.¹ Modification of the naturally complex structures may lead to novel or more potent therapeutics. One modification pathway is hydroaminoalkylation, the addition of an amine across a carbon—carbon double or olefinic bond; the Schafer group has developed a family of catalysts for such reactions.² In our earliest

work, we demonstrated the addition of N-methylaniline (NMA) to β -pinene and limonene using our tantalum-catalyst (Fig. 1). In this report, we describe amination of turpentine (provided by Holmen Pulp) without added solvent (i.e. neat reaction) and preliminary results from a new collaboration with the Page lab (UBC Pharmaceutical Sciences).

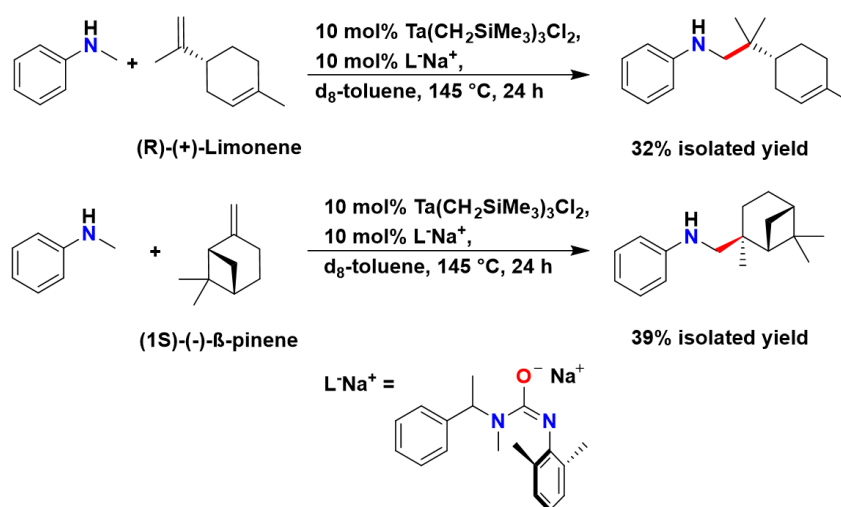


Figure 1. Reaction scheme for β -pinene and limonene amination by hydroaminoalkylation.³

Catalytic transformation of turpentine with and without added solvent

Turpentine was previously determined to contain 57 mol% α -pinene, 26 mol% β -pinene, 9 mol% limonene, and 8 mol% other monoterpenes; only 35 mol% of turpentine (β -pinene and limonene) is reactive with our catalyst. In our previous report, we described and quantified amination of turpentine to produce a mixture of aminated β -pinene and limonene using toluene as a solvent. Toluene was added as a solvent to allow for proper stirring to ensure homogeneity in the reaction mixture. We hypothesized that the non-reactive components of turpentine could serve as solvent during hydroaminoalkylation enabling so-called neat reaction conditions which adheres to the Green Chemistry principle to generate less waste in synthesis.⁴

Methods

Turpentine functionalization with added solvent proceeded with 1 mmol of N-methylaniline (amine) and 1 mmol turpentine

added to a 2 dram vial containing 10 mol% $\text{Ta}(\text{CH}_2\text{SiMe}_3)_3\text{Cl}_2$ and sodium ureate ligand ($\text{L}\cdot\text{Na}^+$) dissolved in 1 mL toluene. The vial was sealed and the reaction was conducted at 145 °C for 24 hours. Turpentine functionalization experiment without added solvent proceeded with 1 mmol of N-methylaniline (amine) added to a 2 dram vial containing 10 mol% $\text{Ta}(\text{CH}_2\text{SiMe}_3)_3\text{Cl}_2$ and sodium ureate ligand ($\text{L}\cdot\text{Na}^+$) dissolved in 1 mmol of turpentine. The vial was sealed and heated to 145 °C for 24 hours.

After reaction completion, the reaction mixture was subjected to vacuum overnight then re-dissolved in 0.8 mL d_8 -toluene and 0.05 mmol of 1,3,5-trimethoxybenzene was added to serve as internal standard. The solution was transferred to an NMR tube for quantitative ^1H NMR. NMR yields were measured in situ without isolation of products; product concentration was calculated with reference to the internal standard.

Results

With toluene as reaction solvent and 10 mol% tantalum catalyst loading, 33% NMR yield of 1 and 60% NMR yield of 2 was achieved from turpentine and N-methylaniline (Fig. 2A). Product 1 is derived from β -pinene and product 2 is derived from limonene. To our delight, the absence of toluene did not hinder the production of 1 and 2 from turpentine. Indeed, 38% NMR yield of 1 and 70% NMR yield of 2 were obtained – higher yields than those obtained using toluene (Fig. 2B). Finally, the aminated products are readily removed from the unreactive turpentine components using acid/base extraction protocols. The observed

increase in reactivity reflects the capability of our catalyst to utilize turpentine also as a solvent without compromised reactivity and to selectively react β -pinene and limonene within a terpene mixture. It should be noted that such catalytic reactions in the Schafer group have been completed on up to 2 kg scale. These results also demonstrate the developments of our catalyst towards a green future by using relatively earth abundant metal catalysts in conjunction with renewable, naturally-sourced materials serving as both reagents and solvent.

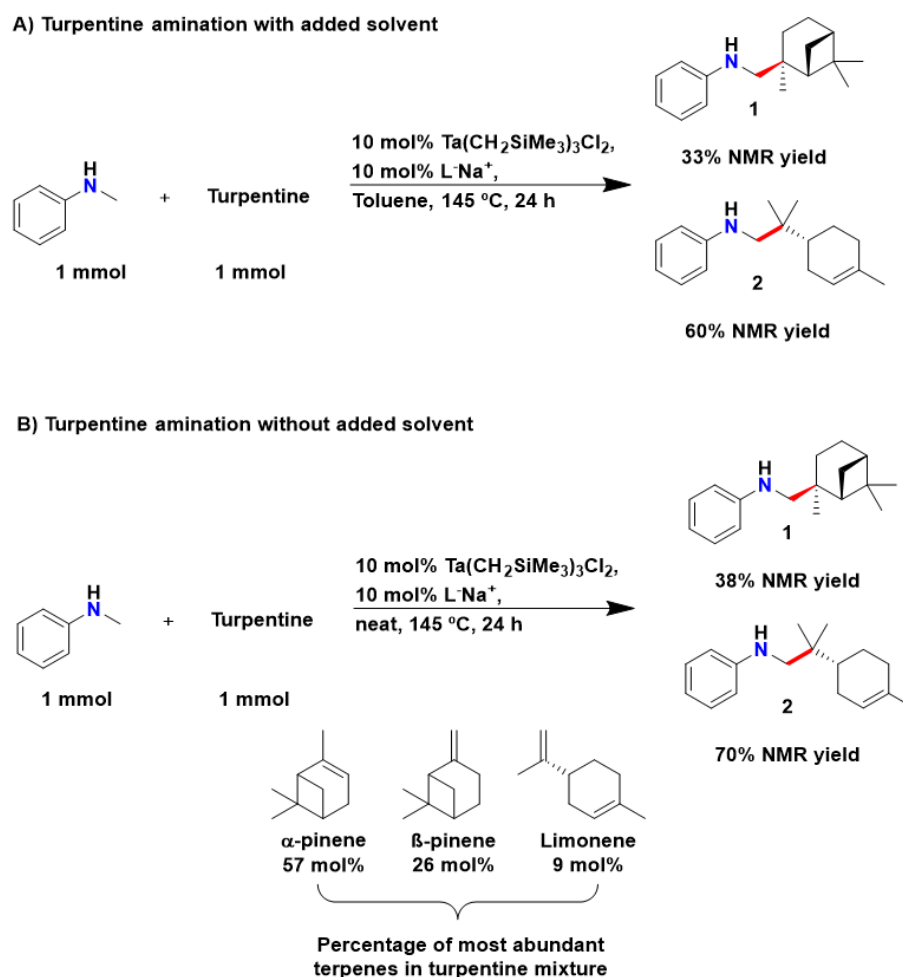


Figure 2. Turpentine amination with toluene as added solvent (A) and without added solvent (B). Product 1 is derived from β -pinene and product 2 is derived from limonene.

In silico screening for anti-mycobacterial activity of aminated terpenes

A new alliance has been established with Dr. Brent Page, Assistant Professor, UBC Pharmaceutical Sciences, and his research associate, Dr. Henok Sahile. The Page Lab specializes in the advancement of compounds towards pre-clinical and clinical testing by identifying and optimizing molecules for disease inhibition. They use computer modeling, a.k.a. in silico tests, to complete an initial evaluation of the ability of molecules to bind and inhibit disease relevant proteins.

Mycobacterium tuberculosis and *Mycobacterium abscessus* are some of the best known disease-causing mycobacterial species. Globally, tuberculosis is the 13th leading cause of death and the second leading infectious killer after COVID-19 (above HIV and AIDS).^{5,6} *M. abscessus* is a common infection in Cystic Fibrosis patients and it is resistant to many currently available antibiotics. Consequently, there is an urgent need to identify new antimycobacterial compounds. Bhattarai et al. (2023) reported the potency of compounds containing a pinene scaffold against mycobacterial pathogens.⁵ The antibacterial activity of these compounds is mediated via inhibition of a protein called Mycobacterial membrane protein Large 3 (MmpL3). MmpL3 is essential for transport of building blocks that are required for

the synthesis of mycobacterial cell wall. Given the structural similarities between compounds reported by DiPucchio et al. (2019)³ and those tested by Bhattari et al. (2023)⁵, in silico tests were conducted to evaluate binding of these compounds to MmpL3.

Methods

Dr. Sahile identified 6 compounds (Fig. 3) in our previous paper (DiPucchio et al., 2019) with structural similarities to Compound 069, the most potent inhibitor reported by Bhattari et al. (2023).^{3,5} The ability of these compounds to bind or dock to MmpL3 (PDB: 6AJG) was modeled using a molecular docking software, GLIDE (Maestro, Schrödinger). MmpL3 participates in the synthesis of bacteria cell walls and is essential to cell replication and viability; inhibition of MmpL3 results in powerful antibacterial activity against *M. tuberculosis* and *M. abscessus*. The performance of pinene-containing molecules was compared to SQ109, a ligand known to be a powerful inhibitor of MmpL3. GLIDE calculates an XPG score which summarizes all favorable and penalizing interactions with MmpL3, where a more negative docking score is considered more favourable.

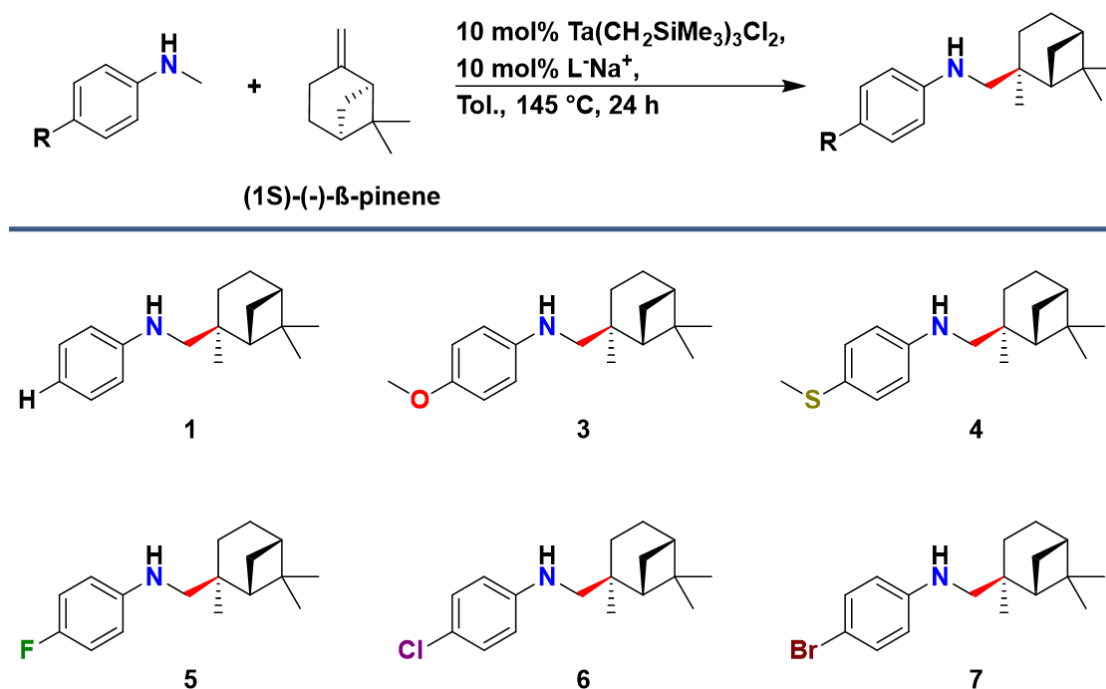


Figure 3. Series of aminated β-pinenes first reported in DiPucchio et al., 2019 and selected for in silico modeling.

Results

Fig. 4 illustrates the binding modes of compound 4, compound 069 Bhattari et al. (2023)⁵ and the reference ligand to the active site MmpL3. The more negative the XPG score, the more medically potent the compound. Typically, potent binding molecules have scores of approximately -10 or less. Higher scores, i.e. closer to 0, could mean that the binding of a compound is weak, the binding modality is unlikely, and/or that the compound could be modified to produce more potent analogues using

medicinal chemistry approaches. SQ109, a baseline molecule for inhibition of MmpL3, has a binding score of -11.4 and the most active compound reported by Bhattari et al. (2023) scored -9.8. Our aminated β -pinenes received XPG scores between -7.5 and -8.2. Compound 4 (Fig. 3) received the lowest XPG score, -8.2, predicting good binding affinity with a similar binding mode and binding pocket or site. The aminated β -pinenes appear to be very promising starting points for medicinal chemistry.

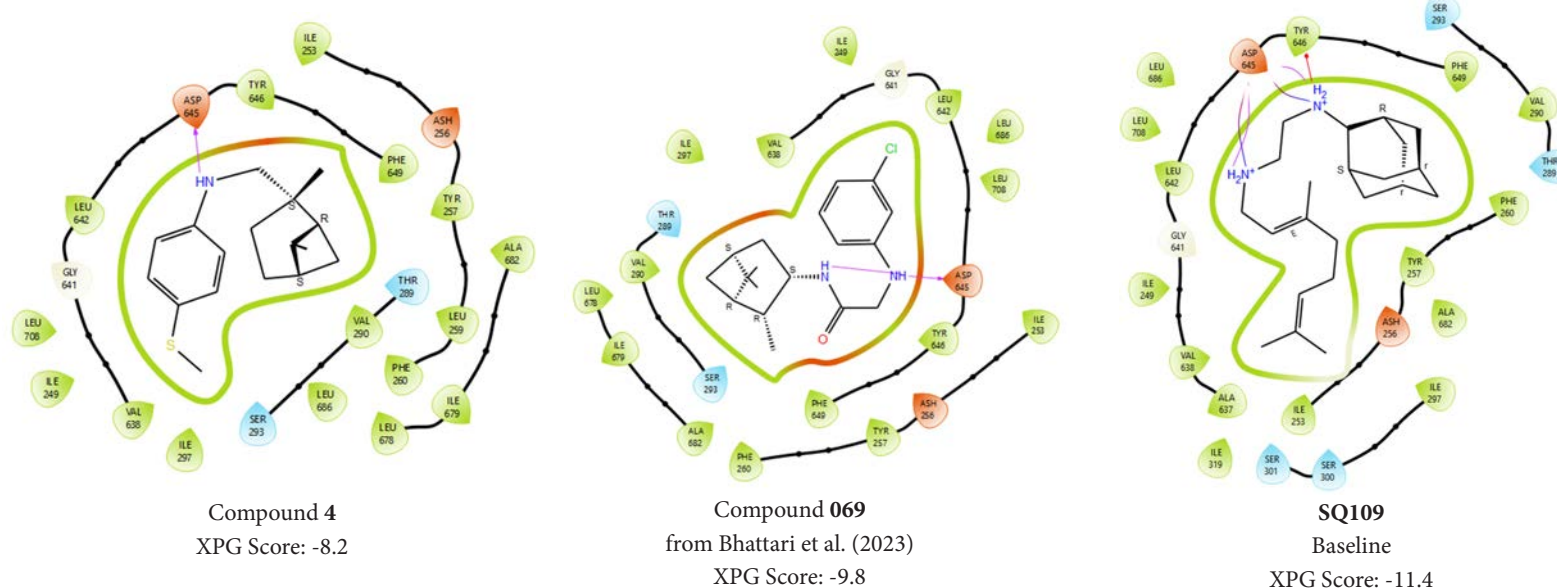


Figure 4. *In silico* docking to MmpL3 by compound 4, compound 069⁵, and SQ109. SQ109 is a well-known potent inhibitor of mycobacterial target protein MmpL3.

Future Research

The product yields from our neat turpentine hydroaminoalkylation reaction is now competitive to the hydroaminoalkylation reactions using commercial sources of β -pinene and limonene in the presence of toluene. The next steps will be to develop a protocol to separate 1 and 2 during product isolation. Standard techniques such as distillation and silica gel chromatography are challenging as 1 and 2 have similar boiling points and molecular polarities.

In vitro screening experiments to test the antibacterial activity of compounds 1 and 3 – 7 against *M. abscessus* and *M. bovis* (BCG), a safer-to-handle surrogate of *M. tuberculosis*, are under way in the Page lab. The results using 1 and 3 – 7 for screening will inspire further structural modifications onto our aminated β -pinenes to increase binding and therapeutic potency. Additional aminated terpenes and turpentine can also be tested in similar assays.

In July 2023, Julianna Lima de Freitas, our previous PhD student, joined Canfor Pulp as Senior Analyst for External Sustainability Reporting. We are currently recruiting an 8-month co-op student for January 2024 to perform linoleic acid recovery from process streams.

References

1. Cox-Georgian, D.; Ramadoss, N.; Dona, C.; Basu, C. *Med. Plants From Farm to Pharm.* 2019, 333–359.
2. DiPucchio, R. C.; Rosca, S.-C.; Schafer, L. L. *J. Am. Chem. Soc.* 2022, 144, 11459–11481.
3. DiPucchio, R. C.; Rosca, S.; Athavan, G.; Schafer, L. L. *ChemCatChem* 2019, 11, 3871–3876.
4. Anastas, P.; Eghbali, N. *Green Chemistry: Principles and Practice.* Chem. Soc. Rev. 2010, 39, 301–312.
5. Bhattarai, P.; Hegde, P.; Li, W.; Prathipati, P. K.; Stevens, C. M.; Yang, L.; Zhou, H.; Pandya, A.; Cunningham, K.; Grissom, J.; Roman Sotelo, M.; Sowards, M.; Calisto, L.; Destache, C. J.; Rocha-Sanchez, S.; Gumbart, J. C.; Zgurskaya, H. I.; Jackson, M.; North, E. J. *J. Med. Chem.* 2023, 66, 170–187.
6. World Health Organization. Tuberculosis Fact Sheet. <https://www.who.int/news-room/fact-sheets/detail/tuberculosis>

PROJECT 2.3

PRODUCTION, CHARACTERIZATION, AND APPLICATIONS OF MFC DERIVED FROM MECHANICAL PULP FINES

Authors: Mariana Frias de Albuquerque, James Olson, Boris Stoeber, Heather Trajano

Background

This project aims to reduce the energy required to produce microfibrillated cellulose (MFC) from mechanical pulp fines for various paper applications through fibre fractionation and the implementation of enzymatic hydrolysis prior to refining.

In a previous phase of this project, we investigated the production of MFC using short fibres obtained from softwood bleached chemi-thermomechanical pulp (BCTMP). The pulp was fractionated using a 0.8 mm hole screen and then refined at the UBC Pulp and Paper Centre pilot plant. The refined short fibres were subsequently combined with long fibres, and paper handsheets were created for mechanical testing. The refined short fibres contributed to the tensile strength of the paper, while the long fibres contributed to the bulk (Seifert et al., 2023) thus bringing us closer to producing high bulk, high tensile papers from mechanical pulp. Furthermore, we have found that the specific refining energy correlates well with the elasticity of fibre suspensions through rheological properties.

At the last ERMP steering committee meeting, we presented the effect of enzymatic hydrolysis of short BCTMP fibres before refining using the PFI mill. We evaluated the effect of pH and hy-

drolysis incubation temperature on post-refining fibre morphology and inter-fibre interactions. High temperature (80°C) softened the structure of the fibres, while high pH (pH 8) modified the surface charge and enhanced the repulsion between fibres. Hydrolysis with cellulases mostly resulted in shorter and less fibrillated fibres. The exception occurred with fibres hydrolyzed with a cocktail of endo- and exoglucanase incubated at pH 8, which showed an increase in the extent of fibrillation. This study was documented in a manuscript and is currently undergoing internal review. Since then, we have investigated the influence of other enzymatic hydrolysis parameters, such as incubation time and enzyme dosage, on fibre morphology post-refining. The results of this study are briefly discussed in this document.

Results

The process parameters for enzymatic hydrolysis of short fibres with endoglucanase (EN) or a mixture of endo- and exoglucanase (EN+EX) before PFI refining are shown in Table 1. These parameters refer to the investigation of the duration of hydrolysis and enzyme dosage.

Table 1. Experimental matrix to assess the effect of incubation time and enzyme dosage on fibre morphology.

	Pulp Consistency (%)	Incubation Temperature (°C)	Incubation pH	Incubation Time (min)	Enzyme Dosage (wt.%*)	Enzyme Type	PFI Revolutions
<i>Incubation time study</i>	3.5	60	5	15	0.0	EN	10,000
				120	0.1		
					1.0		
<i>Enzyme type and dosage study</i>	3.5	60	5	120	0.0	EN	10,000
						EN+EX**	
						1.0	

* Based on the over-dried weight of the pulp

**In the case of the mixture of EN+EX, exoglucanase is an auxiliary enzyme. It is dosed as 10 wt.% of endoglucanases.

The investigation of the exposure time of fibres to enzymes was carried out to evaluate the viability of enzymatic hydrolysis in an industrial mechanical pulping line, where the pulp residence time is less than 20 min. The study of enzyme dosage aims to elucidate the accessibility of fibres to enzymatic action and seek the appropriate dosage of enzymes for generating MFC and MFC-like fibres.

Both investigations evaluate fibre morphology by observing length-weighted fibre length, the extent of fibrillation and the content of coarse and slim fines. These parameters were obtained from the *Fibre Tester L&W+* at Canfor Pulp Innovation (BC, Canada). The extent of fibrillation is associated with the parameter

$$\text{Fibril area (\%)} = \frac{\text{Area}_{\text{fibrils}}}{\text{Area}_{\text{fibre}} + \text{Area}_{\text{fibrils}}} \quad (1)$$

provided by the equipment, calculated from the imaged area of the fibrils $\text{Area}_{\text{fibrils}}$ and the area of the fibres $\text{Area}_{\text{fibres}}$. Coarse and slim fines content are associated with particulate and slender fines, based on a combination of the width and length of the fines particles. The internal method with which the equipment distinguishes the classes of fines is proprietary to the instrument supplier (Hyll, 2016).

Incubation time study

Figure 1 presents the characterization of short fibres that underwent enzyme hydrolysis followed by refining at 10,000 PFI revolutions. Hydrolysis with EN was held at 15 and 120 min, while enzyme dosage ranged from 0 wt.% to 1.0 wt.%.

One of the key observations is a progressive reduction in fibre length with increasing EN dosage. Notably, this fibre shortening effect is significantly more pronounced following a 120-min incubation compared to a 15-min incubation period. Specifically, at 0.1 wt.% dosage, EN leads to a 4% and 8% reduction in fibre length for 15-min and 120-min incubation periods, respectively. The reduction is even more substantial for a 1.0 wt.% dosage, with an 8% reduction in fibre length after 15 min and a substantial 20% reduction after 120 min. There appears to be a trade-off regarding fibre length reduction between time and enzyme dosage. Fibres hydrolyzed with EN at 0.1 wt.% dosage for 120 min exhibit a similar length to those hydrolyzed at 1.0 wt.% for only 15 min. This suggests that an increase in enzyme dosage can compensate for the limitations of a shorter incubation time, emphasizing the importance of enzyme dosage in achieving desired fibre properties.

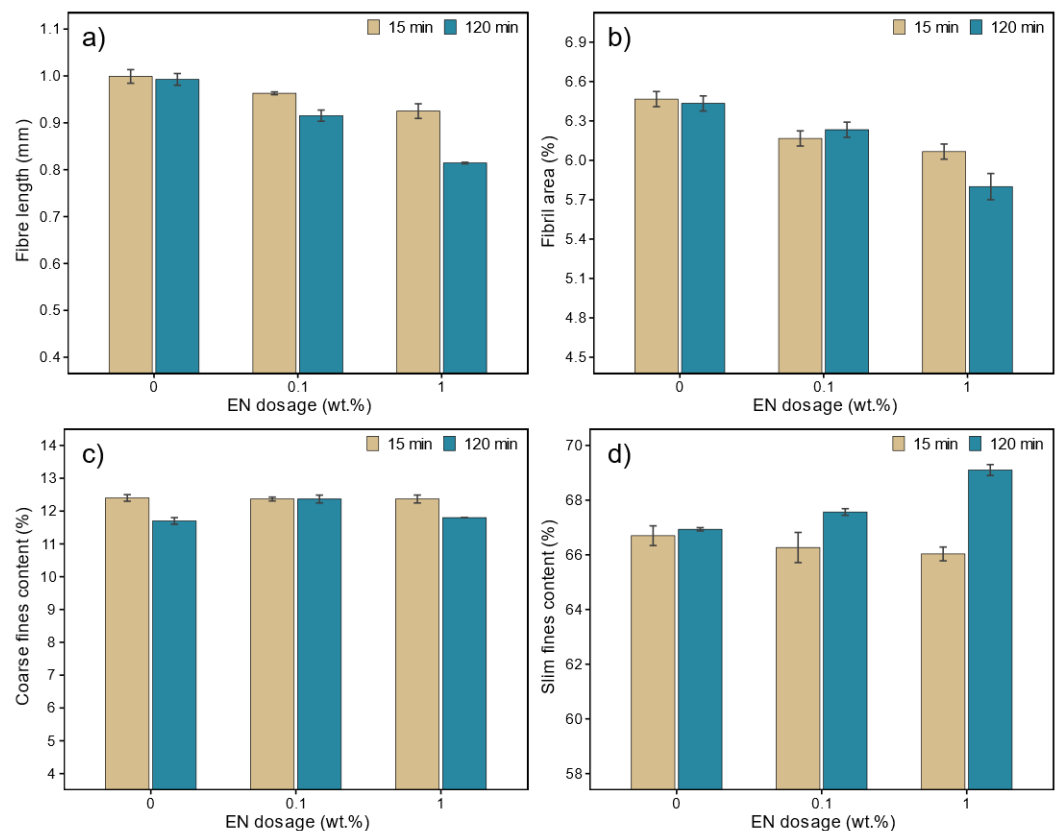


Figure 1. Fibre morphology aspects of refined short BCTMP fibres hydrolyzed with endoglucanase for 15 and 120 min, with enzyme dosage ranging from 0 wt.% to 1.0 wt.% as a compared analysis of (a) length-weighted fibre length, (b) percentage of fibril area, and content of (c) coarse and (d) slim fines.

Furthermore, the reduction in fibril area with increasing enzyme dosage is contrary to the conventional trend of increased fibril area during refining (Kerekes et al., 2023). This can be attributed to the specific mechanisms of EN action and the enhanced accessibility of exposed fibrils within the cell wall to the enzyme (Hildén et al., 2005).

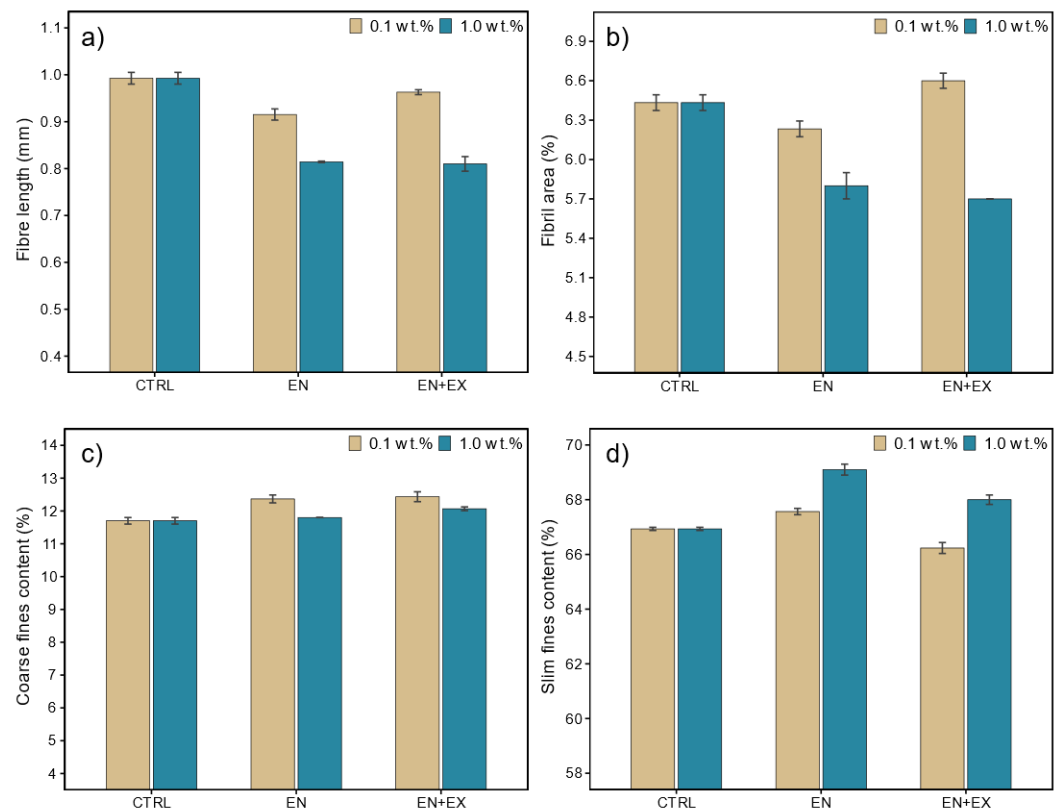
Another aspect to consider is the effect of enzyme hydrolysis on the content of coarse and slim fines. For a 15-min incubation, coarse and slim fines content remain relatively constant with an increase in EN dosage. However, for a 120-min incubation, slim fines content progressively increases with higher enzyme dosages. This difference in fines content suggests that during a 15-min hydrolysis, EN primarily targets exposed fibrils attached

to the fibres, weakening the fibre structure. In contrast, a longer 120-min hydrolysis allows EN more time to interact with the substrate, resulting in greater fibre shortening, fibril detachment, and the generation of slender fines. These findings highlight the complex interplay between enzyme dosage, incubation time, and fibre properties.

Enzyme type and dosage study

Figure 2 presents the characterization of short fibres refined at 10,000 PFI revolutions with or without a pre-hydrolysis step with EN or EN+EX. Hydrolysis was conducted for 120 min, with an enzyme dosage ranging from 0 wt.% to 1.0 wt.%. Exoglucanase is dosed as an auxiliary enzyme, at 10 wt.% of endoglucanase.

Figure 2. Fibre morphology aspects of refined short BCTMP fibres hydrolyzed with enzymes (EN and EN+EX) of dosage ranging from 0 wt.% (CTRL) to 1.0 wt.% as a compared analysis of (a) length-weighted fibre length, (b) percentage of fibril area, and content of (c) coarse and (d) slim fines. In the case of the mixture of EN+EX, exoglucanase is an auxiliary enzyme. It is dosed as 10 wt.% of endoglucanase.



As previously noted, increasing the dosage of EN leads to a progressive decrease in fibre length. Surprisingly, when comparing the impact of EN to EN+EX at 0.1 wt.% dosage, the EN treatment resulted in double the fibre shortening (8% vs. 4%). This discrepancy suggests a potential interaction between EN and EX during hydrolysis at this low dosage, warranting further investigation to elucidate the underlying mechanisms.

Furthermore, adding auxiliary EX at the higher dosage of 1.0 wt.% did not intensify fibre shortening, fibril area reduction, or

coarse fines content generation compared to EN treatment alone. However, it is worth noting that there is a slight difference in the slim fines content. EN+EX generated fewer slender fines than EN. This difference could be attributed to the auxiliary EX's role in partially cutting fibrils attached to the fibres. This action reduces fibril area but produces fines that are too small to be categorized as part of the slim or coarse fines content (the L&W+ has a minimum length detection of 50 μm). These findings shed light on the dynamics of cellulase treatments and their impact on fibre morphology.

Future Research

We will continue investigating the effect of auxiliary enzymes combined with endoglucanase on fibre morphology by including hemicellulases in test cocktails. Additionally, we will evaluate the role of pre-existing mechanical pulp fines on fibre morphology modification by enzyme hydrolysis by including a fines separation step (Britt Dynamic Drainage Jar protocol) before hydrolysis.

Finally, once laboratory-scale tests are completed, we will move on to larger-scale trials using the UBC Pulp and Paper Centre pilot plant's single disc refiner. In these trials, the refining action will be more representative of a mechanical pulping mill, and we can quantify potential energy savings from enzyme hydrolysis.

References

1. Hildén, L., Våljamäe, P., & Johansson, G. (2005). Surface character of pulp fibres studied using endoglucanases. *Journal of Biotechnology*, 118(4), 386–397. <https://doi.org/10.1016/j.jbiotec.2005.05.001>
2. Hyll, K. (2016). Image-based quantitative infrared analysis and microparticle characterisation for pulp and paper applications. KTH Royal Institute of Technology.
3. Kerekes, R., Mcdonald, D., & Meltzer, F. (2023). External Fibrillation of Wood Pulp June 2023. *Tappi Journal*, 22, 363. <https://doi.org/10.32964/TJ22.6.363>
4. Seifert, R., Gharekhani, S., Vargas Figueroa, D., Mercur, J., & Olson, J. (2023). Engineering the paper production by combined fibre fractionation and reinforcement with microfibrillated cellulose. *Cellulose*, 30(5), 3201–3217. <https://doi.org/10.1007/s10570-023-05053-7>

Recent Publications by the ERMP team

1. Ferreira, E. S., Drummond, J., Veiga, A. T., Sibellas, A., Brown, S., Cranston, E. D., & Martinez, D. M. (2023). "Mapping absorbency in cellulosic fibres with iron tracers". *Carbohydrate Polymers*, 311, 120785.
2. Fang, M., Wattoo, E., Palmer, B., Guliov, D., Bicho, P., Cao, Y., Pediredla, V., Gopaluni, B. "Real-time Process Operation Evaluation and Model Reliability Assessment for Chemithermomechanical Pulping Process". *Control Engineering Practice* 138 (2023): 105598.
3. Sibellas, A., Drummond, J., Phillion, A.B. & Martinez, D.M., "Connectivity in Binary Mixture of Spherical Particles", *Powder Technology Journal* (2022). Submitted to *Tomography of Materials and Structures*
4. Brown, S. N. M., Sibellas, A., Drummond, J., Chen, J., Beatson, R., Phillion, A., & Martinez, D. M. (2023). Understanding the origin of micro-compressions in cellulose fibres using 4D X-ray micro-computed tomography, Submitted to *Cellulose*.

PROJECT 3

CREATING BULKY FIBRES AND ADVANCED CHARACTERIZATION THROUGH COMPUTED TOMOGRAPHY

Authors: Anderson Veiga, Lewis Mason, Sam Brown, Elisa Ferreira, Kudzanai Nyamayaro, James Drummond, Emily Cranston, André Phillion, Mark Martinez

Project 3.1 - Enhancing Bulk

The mechanical properties of paper can be enhanced by pulp refining and additives to improve fibre-fibre bonds. Paper strength is typically proportional to the network's density, so high-bulk papers underperform in mechanical testing. In this work, the paradigm of "bulk versus tensile strength" in pulp refining is overcome using applied surface chemistry. In the previous reporting period, a one-step adsorption-based chemical modification was applied to enhance the bulk and resistance of a low-strength pulp (bleached chemi-thermomechanical pulp, CTMP). The chemical modification was performed using hydroxypropylmethylcellulose (HPMC) as a binder that adsorbs irreversibly onto the fibre surface. HPMC is a low-cost, renewable, and food-grade additive derived from cellulose. The hypothesis is that HPMC can reinforce fibre-fibre bonds through polymer entanglement and intermolecular forces. Besides mechanical performance, the adsorption of HPMC on the fibre cell wall is

expected to reduce the interfacial tension inside the lumen, which could potentially prevent the fibre from collapsing due to capillary forces during drying. The key finding is shown in Figure 1 where the tensile strength and bulk increased with both pre- and post-treatments. In this reporting period, we focussed our effort on the characterization of this result in order to understand the physical mechanism. Here, we used computed tomography and characterized the pore size distribution for each treatment. Critically, we find that without treatment, we find the traditional flow-induced compaction of the paper structure near the wire surface (Fig 1, right panel). With treatment, the degree to which densification occurred diminished (Fig 1, right panel) from which we argue that the chemistry stiffened the fibre wall and created more relative bonding through intra-fibre bridging. In the next reporting period, we will examine a wider range of chemical treatments.

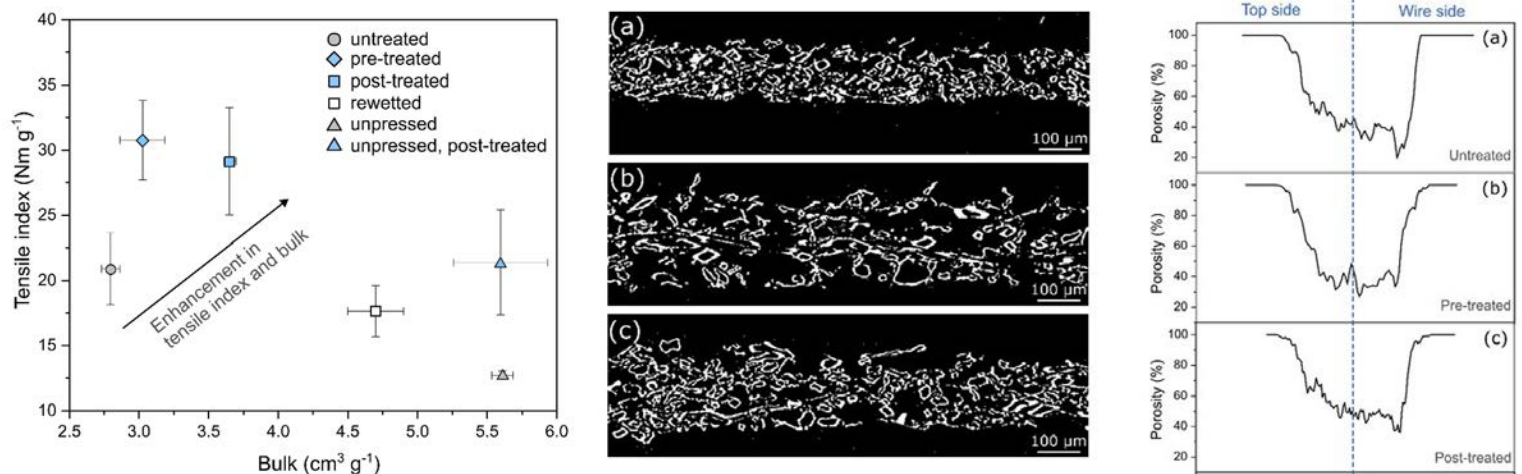


Figure 1. *Left Panel.* Tensile index and the bulk of hand sheets prepared at different conditions: untreated; with 2% HPMC pre-treatment; 2% HPMC post-treatment, unpressed, and rewetted. Samples pre- and post-treated with HPMC exhibited improved tensile index and bulk compared to untreated and unpressed samples. *Right Panel.* Reconstructed μ CT images from hand sheets: (a) control (no additives); (b) pulp pre-treated with 2% HPMC; (c) post-treated with 2% HPMC. The selected cross-sections exhibit a representative morphology of each sample.

PROJECT 3

Project 3.2 - Advanced Characterization

Two activities were conducted in the reporting period: tracer development to enhance contrast in tomography, and, creating a tool to visualize water absorption. Both will be discussed below.

(a) *Tracer development.* In our preceding three newsletters, we reported our iron-labelling protocol for tracers to enhance the visualization of pulp fibres using 3D microscopy. Previous literature has highlighted the efficacy of Co-Fe labelling for fines visualization in handsheets through μ CT. Our contribution is to the successful iron-labelling of not just fines, but also longer pulp fibre fractions. Our previous results indicated that the tensile properties of handsheets were not greatly impacted by the addition of 1 wt.% loading of iron-labelled long fibres in comparison to the same loading of unlabelled fibres. During the last six months, we examined methodologies to segment the images. Both physical and digital approaches were attempted.

In detail, we prepared handsheets with different loadings of iron-labelled fibres – specifically, 0.1, 0.5, 1, and 2 wt.%. X-ray microcomputed tomography (μ CT) was used to visualize the

lowest and highest loadings (see Figure 2, left-panel, left-hand column). In the first part of this experimental campaign, we developed a manual segmentation methodology through the use of an immersion oil (non-drying immersion oil Type HF from Cargille Laboratories, USA) to enhance contrast between the iron-labelled fibres from the unlabelled fibres and the background (air). This is shown in Figure 2, left panel, right column. This approach is promising and iron-labelled fibres can clearly be identified (Figure 3, right-hand column). A second methodology was developed to extract the iron-labelled fibre networks from handsheet samples using machine learning, rather than submerging them in oil. A novel machine learning architecture and its software pipeline were developed to train a neural network (not to be confused with a fibre network) on the visual differences between normal fibres and tracer fibres. The machine learning algorithm can then perform a non-invasive segmentation on the original scans, outputting both the normal fibre network as well as the tracer fibre network. This is shown in Figure 2, right panel.

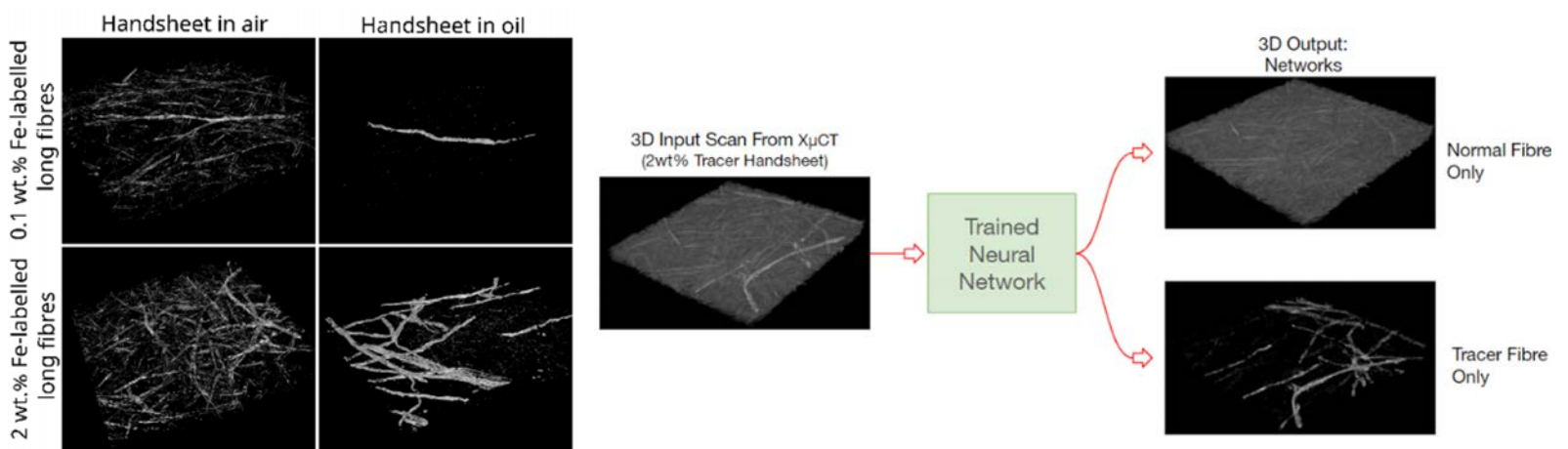


Figure 2. *Left Panel.* μ CT images of BCTMP hand sheets loaded with 0.1 and 2 wt.% iron-labelled long BCTMP fibres, imaged in air (left) and manually segmented to attempt to show only labelled fibres in immersion oil (right). *Right panel.* Trained neural network results demonstrated on the 2wt.% labelled fibre hand sheet. The two outputs from the network are the un-labelled fibre network and the tracer fibre network. *Right Panel.* Trained neural network results demonstrated on the 2wt.% labelled fibre hand sheet. The two outputs from the network are the un-labelled fibre network and the tracer fibre network.

PROJECT 3

(b) *Water Absorption*. Previously, we developed a novel iron tracer chemistry to study the 3D flow pathways of water in paper using 3D X-ray microcomputed tomography. Since the last update, we have made significant progress in our examination of the absorption of liquids in fibrous materials. Driven by the desire to comprehensively characterize commercial hydrophobic paper samples, our current focus is the development of new research methodologies involving the use of macro photography, swept-field laser confocal microscopy, and X-ray radiography. Using macro photography, we quantified the millimetre-scale dynamics of the precursor wetting front in various fabric and paper samples. Using confocal microscopy, we visualized the dynamics of fluorescent dye imbibition at the micrometre scale. The confocal microscopy investigations validated our prior iron tracer findings

by illustrating flow through paper fibres before the filling of external pores (Figure 3, left panel).

Using X-ray radiography, we pioneered a novel method for identifying two wetting fronts in paper. Since X-ray imaging is much more sensitive to subtle changes in density than traditional visible-light-based imaging methods (e.g., macro photography), we are able to identify the presence of a post-wetting front that saturates the paper behind the visible precursor wetting front, as illustrated in Figure 3, right-panel. Work is currently underway to apply these new measurement techniques to gain a deeper understanding of how commercial hydrophobic treatments (e.g., alkyl ketene dimer sizing) affect the physical mechanisms of water absorption at macroscopic and microscopic scales.

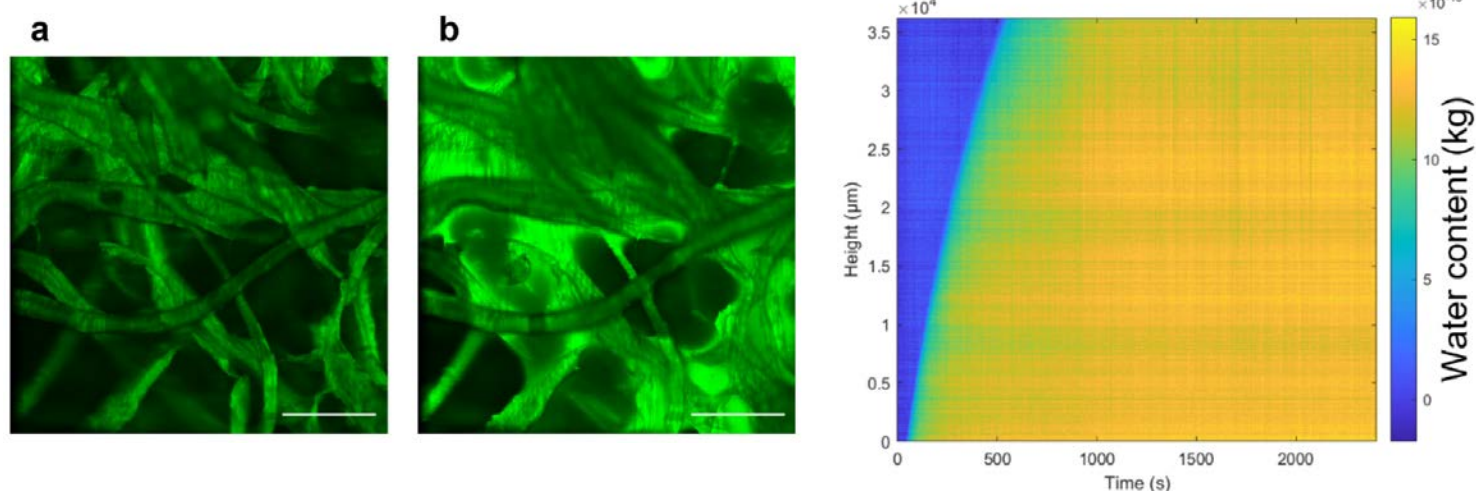


Figure 3. *Left Panel.* Confocal microscope images of blotter paper during the fibre-filling phase (a) and, some time later, the external pore-filling phase (b). Scale bars in both images represent 100 μm. *Right Panel.* Spatiotemporal plot showing the presence of two wetting fronts during water imbibition into paper. Here, the water content of the sheet is measured by X-ray radiography over the height of the sheet and a period of 40 minutes. The light blue line emerging shortly after zero seconds is identified as the precursor wetting front, which separates the dry sheet region (dark blue) from the saturation induced by the post-wetting front (yellow).

Future Research

Our current findings indicate the potential to visualize fibre networks within hand sheets. Of particular interest will be understanding the dispersion and role of NBSK fibres when employed as a reinforcement in mechanical pulp. We recognize the need for an optimized iron-labelling protocol, especially if we aim to enhance scalability. To this end, we are exploring key conditions and how they affect the deposition of iron oxide nanoparticles onto pulp fibres. While our current protocol has proven effective, the diverse nature of fibres and their fractions necessitates further work.

References

1. Hobisch MA, Zabler S, Bardet SM, Zankel A, Nypelö T, Eckhart R, et al. How cellulose nanofibrils and cellulose microparticles impact paper strength—A visualization approach. *Carbohydrate Polymers*. 2021 Feb 15;254.

ERMP PERSONNEL UPDATES

FAREWELLS

We would like to wish the best to our summer undergraduate students, Nilgun Abali, Farah Sadek and Stephen Lee as they provided invaluable support to our ongoing research and trials at the PPC Pilot plant. Their dedication and hard work in working with Projects 1.1 and 2.3 are highly appreciated. We also wish the best to Juliana in her new position in Canfor Pulp as Senior Analyst for External Sustainability Reporting.

Additionally, we are excited to introduce you to the new team members of the ERMP team. We encourage you to take a moment to familiarize yourselves with their backgrounds and read their introductory profiles below.

NEW ARRIVALS

Postdoctoral fellows

Kudzanai Nyamayaro

Dr Kudzanai Nyamayaro received his Ph.D. from the University of British Columbia, UBC. Kudzanai has a passion for sustainability and addressing challenges related to the climate. Kudzanai's PhD research focused on the chemical modification and application of bio-derived and synthetic biodegradable polymers in advanced applications. He is interested in extending his knowledge to pulp and paper products. Kudzanai joined the ERMP program in September 2023 and he will be conducting research on surface modification of mechanical pulp in order to increase the bulk and tensile strength.



COOP students

Oren Han

Oren is a third year mechanical engineering student at UBC. He will be preparing samples and conducting tests for Norman, Fariba, and other researchers who need assistance at the PPC. Oren



wants to gain experience in different industries, and the work in the paper-making lab is his first step. He is excited about all aspects of this job.

Kasish Mahajan

Kasish is a fourth year chemical engineering student at UBC. He is currently a co-op student working in the ERMP program under the supervision of Fariba Yeganeh and Norman Roberts. His role as a co-op student is to assist in ongoing research/projects and involves doing work such as freeness tests, consistency checks, and preparing hand-sheets of varying proportions of components - using both the Tappi procedure and the Dynamic Sheet Former (DSF). He actively engages in research projects which have a key focus on sustainability and enjoys playing music as well. Prior to working at ERMP, Kasish has completed 3 years of studies and 1 co-op work term.



Mitacs Globalink Student

Joanne Wang

Joanne Wang is an undergraduate student from the South China University of Technology, majoring in applied chemistry. She studied the extraction, and modification of pink lignin and its sunscreen skincare performance. It lays a foundation and interest



in the value of forest residues. During the summer of 2023, Joanne joined the ERMP team at UBC. Her project focused on the effect of enzyme types and dosages in hydrolysis incubation on mechanical pulp fiber morphology, as part of Project 2.3. She used BCTMP to do hydrolysis with different dosages and conditions. After that, Joanne tested the fibers' morphology, revealing the correlation mechanism of

enzyme dosage and proportion with the performance of MFC trial production. Joanne really found interesting and meaningful to study under the energy reduction in mechanical pulping program.

ERMP NEWS

Prof. Heather Trajano named Top 10 Under 40 by Pulp & Paper Canada



Congratulations to Professor Heather Trajano for being part of the 2023 Top 10 under 40 by Pulp & Paper Canada. Heather has been an active participant of the consortium since the early stages and leads several projects of the program.

"Heather's recent accomplishments include the demonstration of highly-alkaline peroxide treatment for strength enhancement of mechanical pulps, valorization of extractives while simultaneously reducing water treatment challenges, and patenting an enzyme-LC refining process for surface treatments of paper. Her work is characterized by the application of fundamental engineering principles and careful experimentation to produce a thorough and definitive understanding.

Heather has also adopted a leadership role in the development of EDI policy in the faculty, serving as the benchmark and lens for other units in the university. She has a strong educational portfolio by voluntarily teaching pulp and paper science to new recruits in the industry, as well as the introduction of unit processing in her undergraduate lectures. Nearly a hundred students have participated in her Biomass Fractionation or Sustainable Bioenergy and Biorefinery course offerings." (Pulp & Paper Canada, 2023).

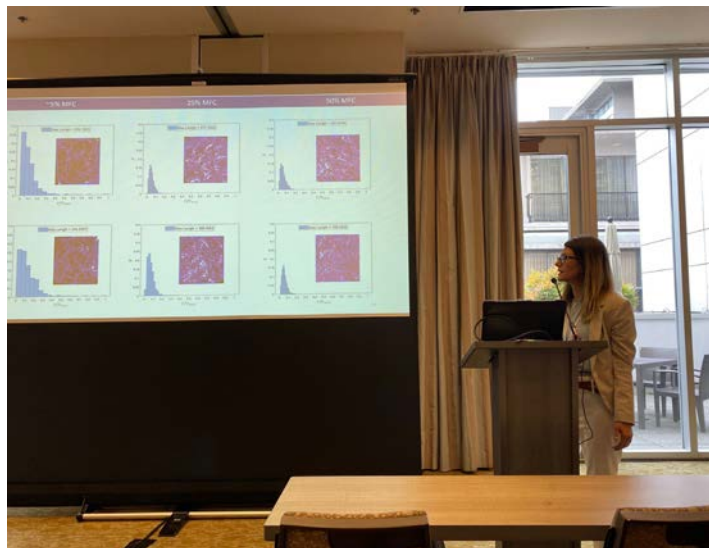
Prof. Emily Cranston elected a member of The College of the Royal Society of Canada

Congratulations to Professor Emily Cranston on being elected a Member of The College of the Royal Society of Canada Class of 2023. Emily joined Phase 3 of the program to bring expertise on surface chemistry, nanocellulose and their application to a range of sustainable bioproducts. She has been awarded the Royal Society of Canada (RSC) Rutherford Memorial Medal in Chemistry established in 1980 for her exceptional research contributions in chemistry.

"Emily is a world-leading nanoscientist and her research is expanding the use of nanocellulose, derived from sustainable bio-based resources like wood pulp, in technologies that offer environmentally-friendly alternatives to petrochemical-based materials and plastics. Emily will be honoured during the RSC Awards Ceremony on November 17, 2023, as part of the 2023 RSC Celebration of Excellence and Engagement". (The Royal Society of Canada 2023 Award Winners).



SHARING OUR RESEARCH



Page 38.

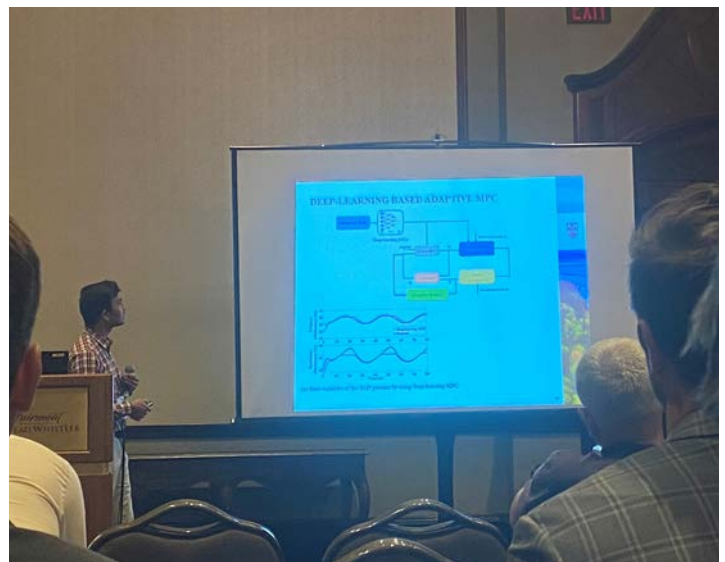
Participation of the ERMP team in different conferences: Top left shows Mariana Frias, Anderson de Veiga and Samira Gharehkhani participating in the TAPPI Nano Conference this summer in Vancouver. The three of them presented part of their work as oral presentations and/or poster presentations. Congratulations to Anderson for receiving the EDI Scholarship!

The bottom right photo shows Mariana presenting her work at the European Polysaccharides Network of Excellence Conference in Graz, Austria this past month.

Page 39.

A short summary of our days at the Whistler PacWest conference and the June ERMP Steering Committee meeting. Top left: Farah Sadek, Gloria Noki, Daniela Vargas Figueroa, Sam Brown, Anderson de Veiga and Mariana Frias. The other pictures show the research presentations by Mariana at the ERMP SCM, and Matthias Aigner and Vijay Kumar at PacWest. Mariana also presented at PacWest and was awarded the best student oral presentation, Congratulations Mariana!

TIME IN WHISTLER



CONTACTS

You are welcome to contact any of the faculty or staff:

Daniela Vargas Figueroa
Program Manager, UBC
604-827-2390
Daniela.Figueroa@ubc.ca

Mark Martinez
Professor, UBC
604-822-8564
Mark.Martinez@ubc.ca

James Olson
Professor, UBC
604-822-5705
James.Olson@ubc.ca

Rodger Beatson
Professor, BCIT
604-432-8951
Rodger_Beatson@bcit.ca

Laurel Schafer
Professor, UBC
604-822-9264
Schafer@chem.ubc.ca

Peter Wild
Professor, UVic
250-721-8901
PWild@uvic.ca

Bhushan Gopaluni
Professor, UBC
604-827-5668
Bhushan.Gopaluni@ubc.ca

Emily Cranston
Professor, UBC
604-827-0627
Emily.Cranston@ubc.ca

Boris Stoeber
Professor, UBC
604-827-5907
Boris.Stoeber@ubc.ca

Heather Trajano
Associate Professor, UBC
604-827-1823
Heather.Trajano@ubc.ca

Yankai Cao
Assistant Professor, UBC
604-822-2693
Yankai.Cao@ubc.ca

Scott Rennekar
Professor, UBC
604-827-0637
Scott.Rennekar@ubc.ca

André Phillion
Professor, McMaster
905-525-9140 x24046
Philliab@mcmaster.ca

Visit our website

www.EnergyReduction.ppc.ubc.ca

PARTNERSHIP IS OUR STRENGTH

The supporting partners of this research program are:

AB Enzymes, Alberta Newsprint Company, BC Hydro, BCIT, Canfor, FPInnovations, Holmen Paper, McMaster University, Millar Western, NSERC, Paper Excellence, The University of British Columbia Pulp and Paper Centre, The University of Victoria, West Fraser and Valmet.

